THESIS FOR THE DEGREE OF DOCTOR OF PHILOSOPHY

Lean NOx reduction over silver-alumina catalysts

Aspects on synthesis, structure and activity

HANNES KANNISTO

Department of Chemical and Biological Engineering

CHALMERS UNIVERSITY OF TECHNOLOGY

Gothenburg, Sweden 2010

Lean NOx reduction over silver-alumina
Aspects on catalyst synthesis, structure and activity
HANNES KANNISTO
ISBN 978-91-7385-445-0

Doktorsavhandlingar vid Chalmers tekniska högskola
Ny serie nr 3126
ISSN 0346-718X

Department of Chemical and Biological Engineering
Chalmers University of Technology
SE-412 96 Gothenburg
Sweden
Telephone + 46 (0)31-772 1000

Cover: NOx conversion vs. temperature over three different silver-alumina catalysts, represented by TEM micrographs. In the background, a monolith washcoated with silver-alumina.

Chalmers Reproservice
Gothenburg, Sweden 2010

Lean NOx reduction over silver-alumina

Aspects on catalyst synthesis, structure and activity

HANNES KANNISTO
Department of Chemical and Biological Engineering
Chalmers University of Technology, Göteborg 2010

Abstract

The aim of this thesis is to increase the understanding of how to design highly active silver-alumina catalysts for selective catalytic reduction of NOx with hydrocarbons (HC-SCR) in oxygen excess at low temperatures (150-250 °C). Silver-alumina catalysts have been prepared using different methods, including a new unique preparation method developed during the thesis project. The obtained catalysts have been thoroughly characterized by a range of methods, to determine the chemical and physical properties. The catalytic performance of the samples was determined using flow reactor experiments and mechanistic aspects of the HC-SCR reaction were elucidated by kinetic modeling and *in-situ* diffuse reflection infra-red Fourier transformed (DRIFT) spectroscopy.

The results show that silver-alumina catalysts with highly dispersed silver can be obtained by the new preparation method based on freeze-drying of the silver-alumina gel, formed by the sol-gel method, presented in this thesis. However, the flow reactor experiments showed that to achieve a high NOx reduction activity at low temperatures, both the nature of the reducing agent and the silver loading of the catalyst must be considered. A delicate balance between the oxidative and reductive properties of the catalyst is required, which in turn is dependent on both the silver loading and the preparation method. This balance varies for different reducing agents, most likely due to the different terminal C-H bond strengths in the hydrocarbons. It is suggested that these two factors determine the rate of partial oxidation, required to open up the HC-SCR reaction path.

A transient kinetic model for hydrogen assisted n-octane-SCR has been developed, using the reduction of stable surface nitrates by hydrogen as a key-step. The model is able to well reproduce changes in the gas feed, especially poisoning effects by higher NO concentrations in the feed. These results, together with *in-situ* DRIFT results showing the reduction of surface nitrates by hydrogen, strongly indicate that one important role of hydrogen is to suppress the self-poisoning of the active sites by reduction of surface nitrates.

Keywords: Lean NO_x reduction, silver-alumina, selective catalytic reduction, HC-SCR, catalyst preparation, freeze-drying, sol-gel, kinetic modeling, aromatic hydrocarbons, characterization, DRIFTS.

.

List of papers

I. *Ag-Al_2O_3 catalysts for lean NO_x reduction - Influence of preparation method and reductant.*
H. Kannisto, H.H. Ingelsten and M. Skoglundh, J. Mol. Catal. A: Chem. **302** (2009) 86

II. *Effect of reductant and catalyst structure on the HC-SCR of NOx over Ag/Al_2O_3 – relationship between hydrocarbon nature and silver loading.*
H. Kannisto, K. Arve, E. Olsson, H.H. Ingelsten, K. Eränen, M. Skoglundh and D.Yu. Murzin, submitted to Journal of Catalysis.

III. *Kinetic modeling of selective catalytic reduction of NO_x with octane over Ag-Al_2O_3.*
D. Creaser, H. Kannisto, J. Sjöblom and H.H. Ingelsten, Appl. Catal. B: Env. **90** (2009) 18

IV. *Aspects of the role of hydrogen in H_2-assisted HC-SCR over Ag-Al_2O_3.*
H. Kannisto, H.H. Ingelsten and M. Skoglundh, Top. Catal. **52** (2009) 1817

V. *H_2 activation of aromatic hydrocarbons over Ag/Al_2O_3 diesel-SCR catalysts.*
H. Kannisto, K. Arve, H.H. Ingelsten, K. Eränen, M. Skoglundh and D.Yu. Murzin, in preparation.

Contribution report

I. I performed all experimental work, interpreted the results together with my co-authors and was responsible for writing the manuscript.

II. I performed the preparation of the samples, the O_2-chemisorption, the bright field TEM analysis and the majority of the activity tests. I also interpreted the results together with my co-authors, especially Kalle Arve and Eva Olsson (STEM analysis), and was responsible for writing the manuscript together with Kalle Arve.

III. I performed all experimental work, interpreted the results with my co-authors and wrote the experimental parts and some of the introduction of the manuscript.

IV. I performed the XPS analysis, interpreted the results together with my co-authors and was responsible for writing the manuscript

V. I performed the preparation of the samples, parts of the activity tests, interpreted the results together with my co-authors, especially Kalle Arve, and was responsible for writing the manuscript together with Kalle Arve.

Papers not included in the thesis

1. *Experimental and theoretical characterization of NOx species on Ag/α-Al_2O_3.*
H.H. Ingelsten, A. Hellman, H. Kannisto and H. Grönbeck, J. Mol. Catal. A: Chem. **314** (2009) 102
2. *Efficient low temperature lean NOx reduction over Ag/Al_2O_3 – Optimization of a possible on-board system.*
H. Kannisto, X. Karatzas, J. Edvardsson, L.J. Pettersson and H.H. Ingelsten, in preparation.

Contents

1 Introduction

In recent years, the awareness of global warming has increased rapidly. Especially the release of the reports by the IPCC (Intergovernmental Panel on Climate Change) working groups during 2007 [1-3] clearly stating that global warming is due to mankind, has contributed to this awareness. The political response to this matter has been massive, as worldwide commitments have been signed, both in the Kyoto protocol [4] and at the Bali conference [5], to reduce the emissions of greenhouse gases. This has induced legislations for reducing harmful emissions from combustion of fossil fuels, rapidly increasing in stringency. Most commonly, the debate is addressing the transport sector, primarily the land-based transports, but now also air- and sea transports [6]. The focus on the transport sector is not because it shows the largest amount of emissions per se, but rather due to the rapid growth of this sector. The regulation of harmful emissions, from primarily land based heavy vehicles such as trucks, is however not a new idea. The first regulations were set already in the 1970's [7], starting with emissions of unburned hydrocarbons (HC) and carbon monoxide (CO). This was quickly followed by regulations of nitrogen oxide (NOx) emissions. To meet these new demands, the three-way catalyst (TWC) was introduced by Volvo in 1978 [8], simultaneously reducing the emissions of NOx, CO and unburned HC with high efficiency. In Sweden, the TWC was introduced on passenger cars of 1989 years model, as a consequence of the emission regulations [9]. However, the TWC is only efficient in a very narrow air-to-fuel ratio, which occurs when the engine is operated at stoichiometric conditions, i.e. as the conventional Otto engine. Using diesel engines, the air-to-fuel ratio is too high for the TWC to efficiently reduce NOx.

As the world becomes increasingly globalized, the need for transports to sustain the demands from the modern society is growing quickly. The total emissions of greenhouse gases from the transport sector in the European Energy Agency (EEA) member countries have increased by 27 % between 1995 and 2005 [6], due to the growth of the transport sector. The recent legislations on reduction of CO_2 emissions have contributed to the development of fuel-efficient engines, however historically primarily the fuel price has acted as the driving force for this development. Nevertheless, the use of fuel-efficient engines has lowered the emissions of anthropogenic CO_2 due to combustion of petroleum based fuel for the individual engine, although this has only diminished the increase in total greenhouse gas emissions. Lean-burn and diesel engines operate at lean conditions (oxygen excess), using the fuel more efficiently than the conventional Otto engine, which operates at stoichiometric conditions [10]. As the fuel is more completely combusted in diesel and lean-burn engines, less fuel is needed, in turn reducing the emissions of CO, CO_2 and unburned hydrocarbons. However, as the exhausts contain a high level of oxygen (around 10 vol.%), the traditional TWC is unable to reduce NOx effectively. This is due to the efficient combustion of HC and CO, which are required to reduce NO_x over the TWC [11], but also the formation of inactive rhodium oxide in the TWC [12].

The term NOx is a collective name for the two nitrogen oxides NO and NO_2, sometimes also including N_2O and other nitrogen oxides [13]. Nitrogen oxide (NO) is harmful to the environment and mankind, *inter alia* by causing ground level ozone, which is one of the components in photochemical smog, and acid rain. [13]. Nitrogen dioxide (NO_2) is directly harmful to humans and animals as it forms nitric acid in contact with water, i.e. in the lungs when inhaled, which may lead to e.g. pulmonary edema [13]. Nitrous oxide (N_2O) is also a

severe greenhouse gas, with about 270-300 times higher global warming potential (GWP) than CO_2 [13, 14]. This has been known for a long time, leading to legislative levels of allowed emissions of NOx. These levels have decreased drastically from the early 70's, from several tens of grams per kilowatt hour to the levels of today, e.g. US10: 0.27 g NOx/kWh [15].

The problem with NO_x emissions from lean combustion calls for more efficient NOx abatement techniques than the traditional TWC. Today, there are several techniques to reduce the NOx emissions from e.g. diesel engines, as exhaust gas recirculation (EGR), NOx storage and reduction (NSR) and selective catalytic reduction (SCR). The EGR technique involves recirculation of parts of the exhaust into the combustion chamber, lowering the flame temperature and oxygen concentration during the combustion. This reduces the formation of NOx, however the reduced oxygen concentration promotes the formation of particulate matter (PM) [16]. NSR requires the engine to cycle between longer periods of lean conditions and short periods of rich (fuel excess) conditions. During the lean period, the NOx is oxidized over platinum and stored as nitrates on a suitable material, commonly barium oxide or barium carbonate [17-19]. When the engine is turned to operate at rich conditions, the nitrates are released and reduced to gaseous nitrogen and water, using CO and unburned HC as reducing agents. However, this technique requires sophisticated engine control and the storage material is very sensitive for sulfur poisoning, deactivating the catalyst. SCR involves adding a urea solution to the exhaust stream, decomposing to ammonia (NH_3-SCR) which in turn reduces the NOx to N_2 and water over a catalyst [20]. These techniques have been commercialized and are applied both for heavy and light duty vehicles. The main technique of this work, hydrocarbon-SCR (HC-SCR), uses hydrocarbons (ideally the fuel itself) as reducing agent, instead of urea. This has a number of advantages, as the infrastructure is already in place and no extra tank for the reducing agent is required. Also, the problem of the water based urea solution freezing at temperatures below -11 °C [21] is avoided. However, there is still much research and development needed to increase the low temperature activity for the HC-SCR system, necessary for light and heavy duty vehicle applications. Nevertheless, a system for E85-SCR was very recently commercialized by General Electric Company, for off-road and train applications [22].

1.1 Objectives

This work has been performed as a part of the E4-Mistra program (Energy Efficient Reduction of Exhaust Emissions from Vehicles), phase 1. The objective of this program is to "demonstrate very low emission levels (0.005 g PM/kWh and 0.1 g NO_x/kWh) with an engine exhibiting low CO_2 emissions" [23]. This should be compared to the current legislative levels: 0.013 g PM/kWh and 0.27 g NOx/kWh in North America (US10) and 0.01 g PM/kWh and 0.4 g NOx/kWh in the European Union (EuroVI, implemented 2013.01) [24].

The aim of this work has been to develop a new type of catalyst for HC-SCR of NOx, demonstrating high NOx reduction with selectivity to N_2 at low temperatures (150-250 °C), to be able to meet the E4 objectives above. The initial approach was to synthesize silver-alumina catalysts by three different preparation methods, including a unique method developed during the thesis project (Paper I). The catalysts were thoroughly characterized and compared with respect to catalytic activity and selectivity for lean NOx reduction, using different reducing agents (Paper I and II), coupling the activity to the silver loading and the nature of the reducing agent.

Small amounts of hydrogen added to the feed results in a remarkable enhancement of the NOx reduction activity over silver-alumina, the so called hydrogen effect (e.g. ref. [25, 26]). However, the role of hydrogen in hydrogen assisted HC-SCR is not yet fully understood. To enhance the understanding of the role of hydrogen and the hydrogen effect several studies were performed (Papers III-V). A global transient kinetic model is presented for the hydrogen assisted selective catalytic reduction of NO_x with n-octane over one of the prepared silver-alumina catalysts (Paper III). The model is based on the removal of surface nitrates by hydrogen as a key feature and offers an explanation for the fast transients in NOx conversion when hydrogen is introduced to the feed. Further evidence for removal of surface nitrates by hydrogen was obtained by *in-situ* DRIFTS experiments (Paper IV) and the influence of hydrogen addition to the HC-SCR reaction, using cyclic and aromatic hydrocarbon reducing agents, is discussed (Paper V).

2 Lean NOx reduction

2.1 The concept of selective catalytic reduction

Selective catalytic reduction is a catalytic reaction, where nitrogen oxides are reduced to nitrogen under lean conditions. This is made possible by the addition of a reductant to the exhaust gases, reacting with the NO_x over the catalyst. The concept of SCR may be divided into ammonia/urea-SCR and hydrocarbon-SCR, referring to the added reductant. The NH_3-SCR technique was introduced in 1957 and has since been used in stationary implementations, to clean the waste gases from e.g. chemical plants and power plants [27]. Research and development for implementation in heavy duty vehicles have been going on for about 20 years [21, 28, 29] and the first applications have been on the market for several years. The NH_3-SCR system has shown excellent catalytic performance [29], but has some major drawbacks as the most common reductant is urea dissolved in water, which thereby may freeze. The most significant drawback however, is that the technique requires a separate tank for the reductant and also a completely new infrastructure for urea. Ammonia is very toxic and harmful for the environment, which makes a clean-up catalyst a necessity to avoid ammonia slip. In HC-SCR the use of hydrocarbons, i.e. fuel, as reducing agent eliminates these problems. There are however other issues to be addressed, concerning this technique.

2.2 The HC-SCR reaction

In the ideal HC-SCR reaction NOx is reduced to gaseous nitrogen in the presence of hydrocarbons and oxygen, simultaneously forming only carbon dioxide and water, as the engine is operating under lean conditions. However, direct combustion of the hydrocarbon reductant will also occur to some extent, depending on the reaction conditions and also on the type of catalyst.

$$NO_x + HC + O_2 \nrightarrow N_2 + CO_2 + H_2O \qquad (1)$$

$$HC + O_2 \nrightarrow CO_2 + H_2O \qquad (2)$$

Competing reactions during HC-SCR: (1) the ideal HC-SCR reaction and (2) direct combustion of the reductant. Both reactions are unbalanced.

The concept of HC-SCR was first introduced in 1990 by Iwamoto et al. [30] and Held et al. [31], independently showing enhanced lean NOx reduction over Cu-ZSM5 zeolites in the presence of hydrocarbons. Platinum group metal (PGM) based catalysts were shortly after shown to be useful as HC-SCR catalysts by Hamada et al. [32] and Obuchi et al. [33], using hydrocarbons present in the exhausts, e.g. propene and propane. The PGM catalysts are effective at low temperatures (below 300 °C), however they have been shown to be selective towards N_2O [34] (and references herein). Since the publications of these findings, several reports have been published on this matter, see e.g. reviews by Burch and coworkers [17, 26, 34] or Liu and Woo [20].

2.3 The silver-alumina catalyst

In 1993, Miyadera presented the silver-alumina catalyst for HC-SCR, showing exceptional activity for reduction of NO under lean conditions in presence of water vapor [35]. As a by-product from combustion of the fuel, water is present in high concentrations in exhausts from combustion engines, and e.g. the Cu-zeolite catalysts presented by Iwamoto et al. [30] and Held et al. [31] were shown to have low hydrothermal stability [29]. The findings by Miyadera [35] made the silver-alumina catalyst an interesting candidate for automotive applications and many studies have been presented in the last 15 years, e.g. structural investigations of the silver-alumina catalyst [36-57] and mechanistic studies of the SCR reaction over silver-alumina [54, 58-91], together with studies on the stability towards sulfur oxides present in the exhausts [5, 80, 88, 92-101]. Also silver-alumina catalysts doped with various noble metals have been presented [100-109]. Later studies have shown that the presence of water in the exhaust actually can be beneficial for the SCR reaction over silver-alumina, using long hydrocarbons as reductant [90].

2.3.1 Influence of the reducing agent

The choice of the hydrocarbon used as the reducing agent for the SCR reaction has a significant impact on the NOx reduction of the catalyst. Long hydrocarbons, i.e. hydrocarbons with a chain length of ca 6-12 carbon atoms, have been shown to shift the activity window of the NOx reduction towards lower temperatures, compared to shorter hydrocarbons, e.g. [90]. Partially oxidized hydrocarbons have also been shown to achieve the same result [35, 110]. However, even if the NOx reduction is shifted towards lower temperature, high NOx reduction is not reached below ca 300°C for non-oxygenated hydrocarbons, which are used as model for diesel fuel. This is a problem, since diesel exhausts are often cooler than 300°C, due to the excess amount of air present during the combustion. On the other hand, the selectivity towards N_2 is high for low-loaded silver-alumina catalysts using non-oxygenated hydrocarbons as reducing agents [34, 78], while a high loading of silver [34, 78] or the use of ethanol as reducing agent [110] has been reported to show higher formation of the undesired by-product N_2O.

2.3.2 The hydrogen effect

In the year 2000, Satokawa [25] reported a remarkable effect on the propane-SCR reaction over silver-alumina by the addition of trace amounts of hydrogen to the feed. The addition of small amounts of hydrogen remarkably increases the low temperature activity for the reduction of NO_x with hydrocarbons under lean conditions. The results presented by Satokawa have been confirmed (e.g. in refs. [111-113]) and also reported to apply for other hydrocarbons as e.g. octane [42, 111]. This effect is shown in Figure 1 for various hydrocarbons as reducing agents.

The increase in low temperature activity is directly dependent on the addition of hydrogen, showing a sharp increase in activity at the time of addition, followed by an equally sharp decrease at the time of removal of the hydrogen. The effect is also repeatable, regaining high activity if the hydrogen is introduced again. However, the hydrogen does not act as a reductant, but rather promotes the SCR reaction [112, 114]. The mechanism behind this promotional effect is however not completely understood, even though many proposals have been put forward about the role of hydrogen [26, 62, 64, 67, 83, 111, 113, 115-118]: removing reaction inhibitors on the catalyst surface [62, 64, 83, 111, 116-118], promoting the partial oxidation of the reductant [67, 115, 116], but also promoting the formation of gas phase species important for the SCR reaction [67]. Furthermore, hydrogen has been proposed to affect the

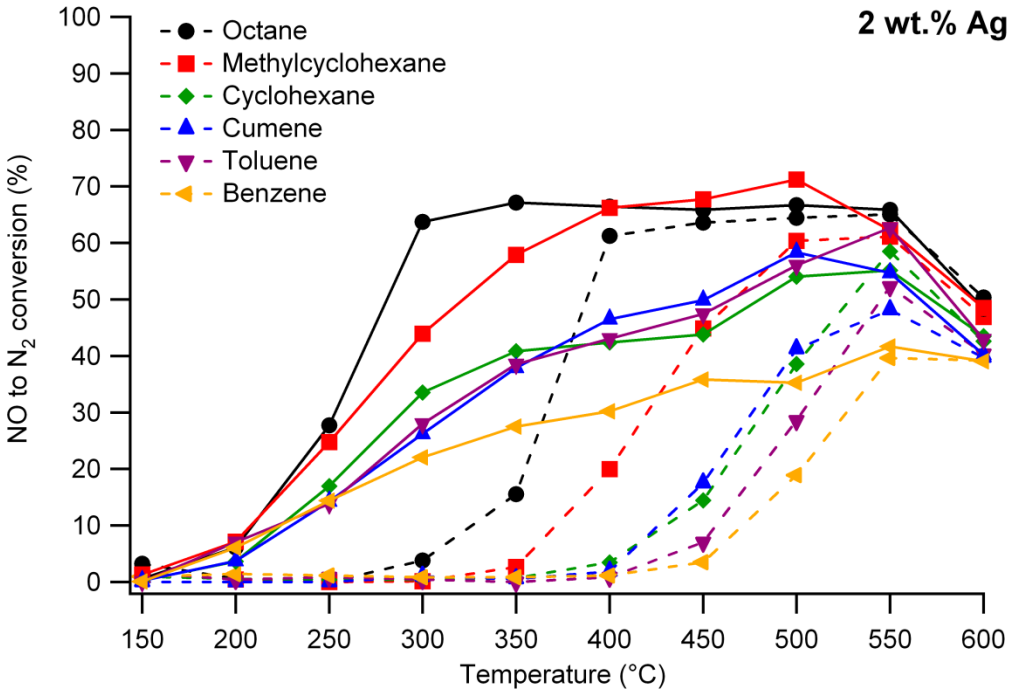

Figure 1: Effect of addition of 1000 ppm hydrogen to the feed for various hydrocarbons over a 2 wt.% silver-alumina catalyst. Dashed lines: without hydrogen addition. Filled lines: with hydrogen addition. Gas feed: 500 ppm NO, 0 or 1000 ppm H_2, 6 vol.% O_2, 10 vol.% CO_2, 350 ppm CO, 12 vol.% H_2O, He bal. C/N=6. Total flow: 500 ml/min. GHSV = 60 000 h^{-1}. See Paper V for further details.

chemical state of silver [26, 64, 83, 113, 117]. In this thesis, attempts have been made to elucidate some of these proposals (Paper III-V)

3 Experimental section

3.1 Catalyst preparation

Silver-alumina catalysts are commonly prepared by impregnation of an alumina support with silver. The method makes it easy to control the amount of active material loaded onto the support, however the dispersion of silver is more difficult to control, especially at higher loadings (see e.g. Paper I). Another way of preparation is by a sol-gel method, where initially an aluminum hydroxide sol is prepared and mixed with a solution of the silver precursor. Although the amount of active material in the final sample may be somewhat more difficult to control, a higher silver dispersion is often achieved (see details below). The catalysts used in this work were prepared according to three different routes, presented in detail in Paper I. Figure 1 describes these preparation methods.

3.1.1 Impregnation

This preparation method is very common for a wide range of supported catalysts. A precursor of the catalytic material, e.g. $AgNO_3$, is dissolved in a solvent and the support, commonly a metal oxide, is immersed in the solution, with or without addition of complex forming agents to facilitate charge attractive forces between the silver complex and the alumina surface. If the conditions (i.e. pH, temperature etc.) are appropriate, the precursor will adsorb onto the support when the solvent is removed. The precursor is then transformed to the catalytic material, possibly reacting with the support, during calcination, i.e. heating in air. The optimum loading of silver for impregnated silver-alumina catalysts is reported to be around 2 wt% [46, 54, 78, 119] .

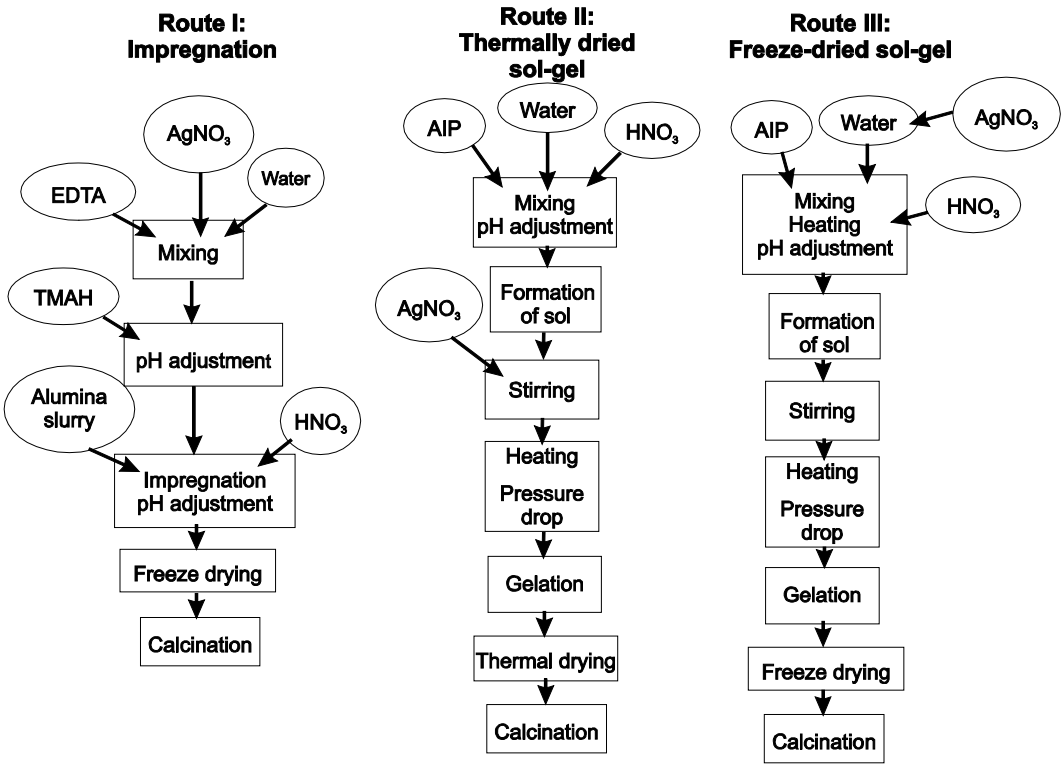

Figure 2: Preparation routes of the silver-alumina catalysts.

3.1.2 Sol-gel

A sol is a liquid suspension of solid particles, where the particles are prevented from sedimentation by the Brownian motion of the water molecules. The very small, solid particles in the sol may be impregnated by a solution of a precursor of the active material. Ideally, this should lead to a higher dispersion of the catalytic material throughout the support matrix. A gel may be formed if a three-dimensional network is established between the particles in the sol. The gel structure keeps the impregnated particles apart while the remaining solvent is removed during drying. Calcination of the dried gel ensures highly distributed catalytic material throughout the support matrix, in contrast to impregnation where the catalytic material is concentrated to the surface of the support material. This is shown in Figure 2, below. In this work an aluminum oxide hydroxide (boehmite) sol was formed by hydrolysis of aluminum isopropoxide (AIP) in water, using silver nitrate as silver precursor.

3.1.3 Freeze-drying

The aluminum hydroxide gel has a very porous structure, resulting in a high surface area. This means that the dispersion of the active material in the gel structure is high, which facilitates a high number of active sites. The porous gel structure may nevertheless collapse during the drying process, resulting in a considerably lower surface area. Freeze-drying of the gel preserves the pore structure of the sample to a higher degree than thermal drying. This is because the high compressing forces over pores with small diameter during evaporation of the water in the gel are avoided by the sublimation of ice [120]. Further, and more importantly, the freeze-drying procedure also prevents agglomeration of silver, as weakly bound silver ions or complexes are fixated by the ice, likely minimizing the formation of metallic silver in the samples prepared by the freeze-dried sol-gel method [121].

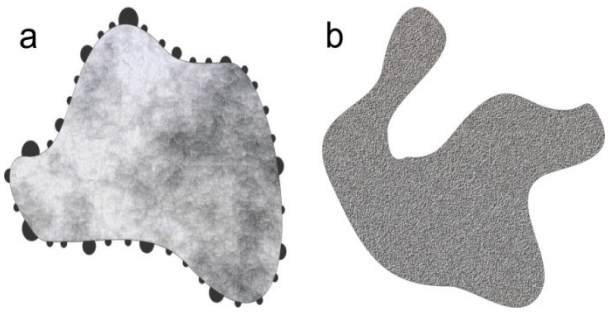

Figure 3: Schematic overview of the distribution of catalytic material in the support of a sample prepared by a) impregnation and b) sol-gel.

3.2 Flow reactor experiments

3.2.1 Monolith reactor

The flow reactor system used for evaluation of the catalytic performance of the samples in Paper I and III has been described in detail previously [122, 123]. In Figure 3, a schematic overview of the system is shown. The reactor consisted of a horizontal quartz tube heated by a heating coil, where the temperature was measured by two thermocouples (type K), 15 mm before the sample and inside the monolith sample (just before the rear end), respectively. The inlet gas composition was controlled by an Environics 2000 gas mixer. The reactor outlet gas composition was analyzed with respect to total NOx, NO and NO_2 by an MKS 2000 FTIR instrument and a 700 EL ht chemiluminescense NOx detector (Eco Physics). The N_2O content was analyzed by the MKS 2000 FTIR instrument and the CO_2 content was measured by an UNOR 610 non-dispersive IR CO_2 analyzer (Maihak). n-Octane was introduced to the reactor via an external CEM-system (controlled evaporator mixer; Bronkhorst), where the octane and carrier gas flows were controlled by mass flow controllers and then mixed at constant temperature (25°C). Further details are found in Paper I and III.

3.2.2 Powder reactor

In Paper II and V, a powder reactor setup, presented in detail in ref. [124] (Figure 5), was used for the evaluation of the catalytic performance. The crushed and sieved (0.4 g, 250−500 µm) catalyst samples were mounted in a fixed bed quartz micro-reactor, which was inserted in an oven equipped with a temperature controller. All the gases were of high purity (AGA) and were introduced into the reactor by means of mass flow controllers (Brooks 5850). Liquid hydrocarbons were added via a syringe pump (CMA 102/Microdialysis). The effluent gas was analyzed by a chemiluminescence NOx analyzer (API model 200AH) and a gas chromatograph (HP 6890 series) equipped with a GS Q column, a GS Molesieve column (J&W Scientific), and FI as well as TC detectors. High purity calibration gases (AGA) were used for calibration of the NOx analyzer and the gas chromatograph. Further details are presented in Paper II and V.

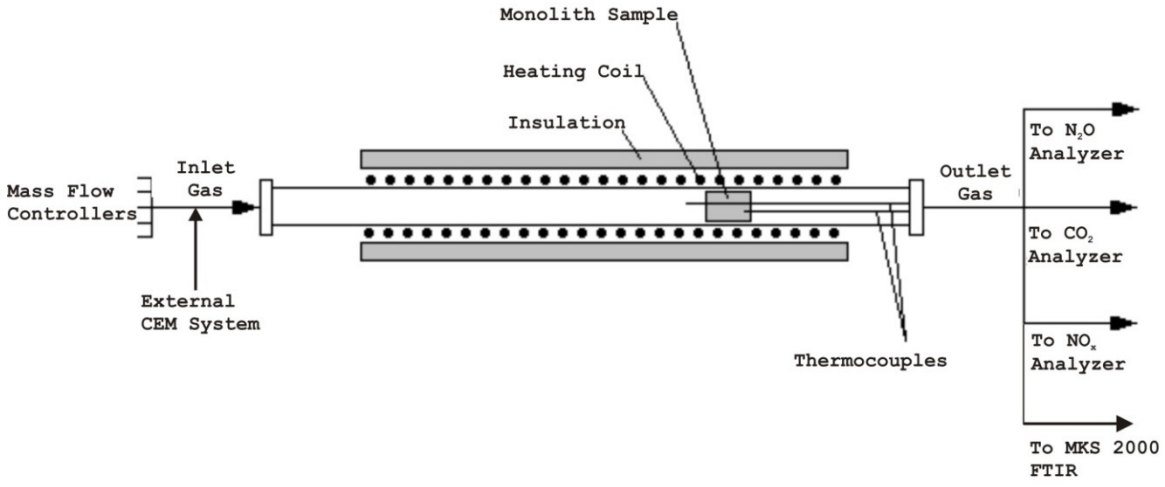

Figure 4: Schematic overview of the monolith flow reactor system used in Paper I and III for performing transient and steady-state experiments.

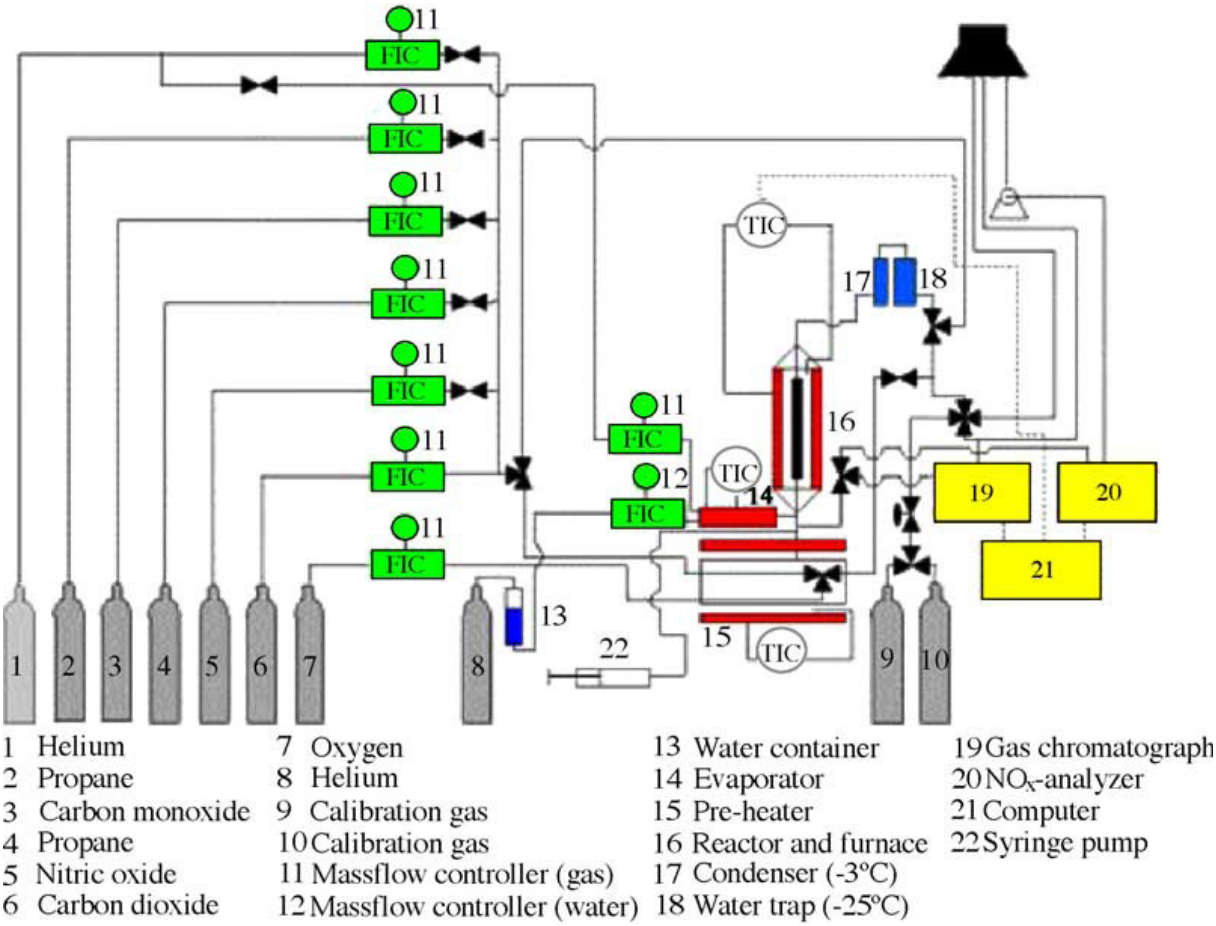

Figure 5: Schematic overview of the powder reactor system used in Paper II and V [124].

3.3 Catalyst characterization

The importance of a thorough characterization of the catalytic sample cannot be stressed enough. To be able to understand the principles behind a catalytic reaction, it is crucial to know the chemical and physical properties of the catalyst. The methods containing the most valuable information are the *in-situ* or *operando* techniques, where the measurements are performed in or close to operating conditions. However, such methods may be very difficult to use. Fortunately, *ex-situ* methods can also provide very useful information about the physiochemical properties of the catalyst.

In the following chapters the methods used for characterization of the different silver-alumina samples are described. Please refer to Paper I-V for thorough details on the methods used in each study.

3.3.1 Nitrogen physisorption

To determine the specific surface area and the pore-size distribution (PSD) of porous materials, such as the catalysts prepared in this thesis project, a common method is to use nitrogen physisorption [125, 126]. A sample tube, containing the degassed sample of known weight, is immersed into liquid nitrogen (77 K) and exposed to gaseous nitrogen at increasing relative pressures p/p_0 from 0 to 1. The gas molecules weakly adsorb on the sample surface, in increasing amount for every pressure step, which may be calculated by the ideal gas law. At a

certain partial pressure, capillary condensation is initiated, shown as a sharp increase in the adsorption isotherm. Increasing the partial pressure allows more nitrogen molecules to adsorb, until bulk condensation is reached. For determination of the specific surface area, the low pressure region of the adsorption isotherm (i.e. increasing p/p_0), typically p/p_0=0.05-0.2, is used, and the BET method [127] is commonly applied. The PSD of the studied material can be calculated from the adsorption branch or the desorption branch (i.e. increasing and decreasing of the p/p_0 ratio, respectively) of the isotherm, usually by the BJH-method [128] which is a combination of the Kelvin equation (Eq. 3) and the Halsey empirical equation (Eq. 4).

3.3.2 X-ray diffraction

X-ray diffraction is in this thesis used for characterization of crystalline phases of the samples. It could also be used for calculating mean particle size or, together with TEM characterization, to indicate particle size differences [129]. This can be achieved since very small crystalline particles or amorphous phases broadens the diffraction peaks or show no diffraction patterns at all. In an X-ray diffractometer an anode, usually consisting of metallic copper, is bombarded with electrons. By this, some of the copper atoms in the anode become excited. When the excited electrons return to the ground state, energy is released as X-ray photons. These X-ray photons are focused in a beam onto the sample to be characterized. When the photons hit the sample they will scatter and this scattering is dependent on the electron clouds surrounding the atoms or molecules of the sample. In certain directions the scattered X-ray waves will interfere and be in phase, the directions determined by the wavelength of the X-ray and the sample crystallinity. Different crystal structures have individual angles of the crystal planes. By changing the incident angle of the X-rays, a diffraction pattern can be achieved, which is unique for the analyzed material. As the crystal structure of the material is analyzed, the obtained diffraction pattern contains information about the bulk of the material.

3.3.3 X-ray photoelectron spectroscopy

X-ray photoelectron spectroscopy (XPS) is used for determination of the elemental composition of the surface of a material and, most important for this thesis, the chemical state of the elements on the sample surface [130]. Monochromatic X-ray radiation is used to ionize the elements of the surface of the sample, releasing photoelectrons. The emitted electrons from these elements are analyzed with respect to number and energy. This method is very surface sensitive, as only electrons from surface elements in the first few atomic layers reach the electron detector. Electrons from deeper atomic layers are reabsorbed by the outer layers of the material. As an electron is emitted from the surface, its kinetic energy may be measured and the binding energy (BE) can be calculated. The binding energy is specific for each element, but is also shifted due to the chemical state of the element. As the photoelectrons are easily absorbed by surrounding gas, measurements are performed at ultra-high vacuum (UHV) conditions, to allow as many photoelectrons as possible to reach the electron detector.

3.3.4 Electron microscopy

Electron microscopy is used for imaging of very small structures, e.g. for determination of the size and shape of supported particles (Paper I and Paper II). This is thanks to the electrons having characteristic wavelengths of less than 1 Å, making it possible to achieve atomic level resolution for modern instruments [131, 132].

A general electron microscope is composed of an electron gun and several sets of lenses; condenser lenses to focus the electron beam and objective lenses to magnify the image generated by the scattered electrons. The resolution of a transmission electron microscope (TEM) is in general equal to or less than 0.5 nm, ensuring images at large magnifications with high quality [132, 133].

The electron beam consists of electrons, accelerated in high vacuum at voltages between 100–400 kV and let through the sample specimen, which should be 100–200 nm thick. Due to the very narrow focus depth, the specimen should also be free from contaminants and have a smooth and flat surface. Diffraction data is achievable, as the electrons transmit the sample. By obtaining the electron image from the central point, a bright field image is obtained. An image obtained from one of the diffracted spots gives instead a dark field image. Both imaging techniques have been used in this thesis.

Scanning electron microscopy (SEM) and scanning transmission electron microscopy (STEM) was used in Paper II and V. The SEM microscope is constructed in much the same way as the TEM, however the image is obtained by rastering a narrow, convergent electron beam and detecting the secondary and backscattered electrons (electrons that "bounces" on the sample), instead of irradiating the sample with parallel beams. This gives a topographic image of the sample, as areas of the sample facing towards the beam will become brighter and areas facing away will appear darker [133, 134]. X-rays emitted from the sample may also be collected and analyzed by energy dispersive X-ray analysis (EDX), giving information of the elemental composition of the sample[133].

STEM combines the SEM and TEM techniques, scanning the sample with a converged beam and detecting the transmitted electrons [133, 134]. By detecting the transmitted electrons, the diffraction of these electrons may be analyzed. Using a high angle annular dark field (HAADF) detector to analyze highly diffracted electrons, the contrast between heavier and lighter elements is increased [132]. This is because heavier elements diffract the electrons to a larger extent than lighter elements. In combination, STEM/HAADF enables very high resolution at an Ångström level [132].

Because the data obtained by TEM and STEM is generated from a very small area, the quality and representativeness of the specimen is crucial. Therefore, the preparation of the sample is a very important step to achieve the desired level of quality. Since dealing with solid material, a small amount is thoroughly crushed in a mortar and dispersed in ethanol. A drop of this dispersion is then placed on the sample holder, a carbon sputtered TEM copper grid. For the SEM/EDX analysis, sample powders of a much larger volume than for the TEM and STEM analyses were placed directly on a solid sample holder, as no transmitted electrons were detected by this technique.

3.3.5 O_2-chemisorption

Chemisorption of different gases is a common way of determining the area of the active metal in a supported catalyst. A classic example is the chemisorption of CO onto platinum. The procedure is very similar to the physisorption used for determining the total surface area of the catalyst. However, in the case of chemisorption, the probe gas interacts more strongly with the material and should thus adsorb selectively onto the desired material. In most cases, the desired material is the active metal of the catalyst. As the amount of adsorbed gas and the

area of the adsorbed molecule is known, it is possible to calculate the accessible metal surface area in the same way as for the nitrogen physisorption (chapter 3.3.1). Given that the loading of the metal on the support is known, the global dispersion and mean particle size of the metal may also be determined.

For the silver-alumina system, chemisorption methods have been unreliable. This is likely due to the differences in the chemical state of the highly dispersed silver in the catalyst samples (see e.g. Paper I and II), which effect the stoichiometry between the metal and the adsorbing gas. Another problem is the tendency for the probe gases to adsorb on the alumina support as well as on the silver. O_2-chemisorption has been put forward as an alternative, as it applicable for metallic silver, but the method is still under development. A thorough discussion about these issues is presented in Paper II.

3.3.6 Diffuse reflectance infra-red Fourier transformed spectroscopy

Fourier transformed infra-red (FTIR) techniques uses the ability of molecules to absorb photons. When a photon is absorbed by a molecule, the molecule gains energy (becomes exited) causing it to vibrate. The energy difference between the vibrational states is dependent on the type of bond and the masses of the atoms in the molecule. Hence, the energy difference is characteristic for the different bonds in the molecule. By irradiating a sample with infra-red radiation it is possible to obtain a spectrum over the unabsorbed IR photons as a function of photon energy, usually given as wave number or frequency. This IR spectrum contains information of the vibrational structure of the sample [133, 135]. However, only molecules where the dipole moment is changed due to the change in vibrations may be detected by this technique, which means that molecules containing polar bonds are readily detected, while molecules lacking a dipole moment are not visible.

In diffuse reflectance infra-red Fourier transformed spectroscopy (DRIFTS) the sample is irradiated by infra-red light and the diffusively reflected radiation is collected by parabolic mirrors (Figure 6). It is then possible to qualitatively measure the vibrational modes of the species adsorbed on the surface of the sample, which may be inhomogeneous (e.g. powder). In combination with the ability of flowing gases over the samples and controlling the temperature, replicating the reaction conditions (*in-situ* measurements), this technique is very useful for investigations of surface reactions occurring in heterogeneous catalysis.

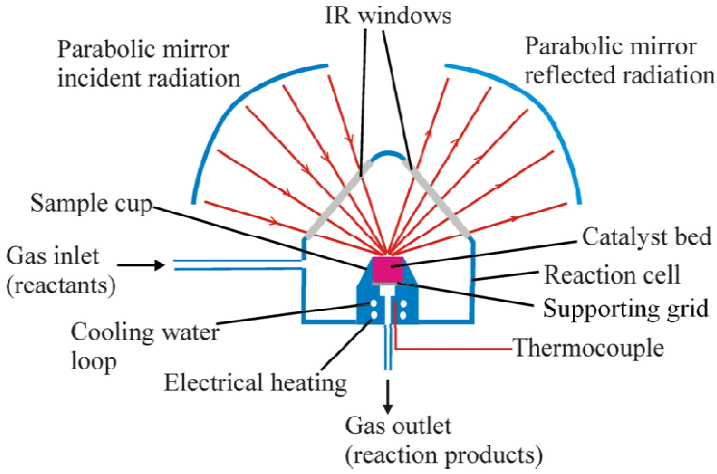

Figure 6: Schematic illustration of the DRIFT cell.

4 Modeling of reaction kinetics

Transient flow reactor experiments were performed to form a base for a kinetic model for the hydrogen promoted HC-SCR reaction over silver-alumina (Paper III). The experiments were performed in the reactor system described in chapter 2.2 above, with a catalytic monolith sample prepared by the thermally dried sol-gel technique (SG5), which is characterized in detail in Paper I. The inlet gas conditions are presented in Table 1 in Paper III.

4.1 Reactor model

The model of the monolithic catalyst may be characterized as follows: the parallel channels in the monolith were assumed identical and axially modeled as a series of 15 continuously stirred tank reactors. Mass and heat transfer from the gas to the washcoat surface were modeled by a film model, where the mass and heat transfer coefficients were estimated from a Sherwood/Nusselt number correlation and the mass transport resistance in the washcoat was neglected. The low concentrations of the reactant species allowed the assumption of constant total mole flow, with respect to reactions between the reactant species. However, the influence of temperature variation on the total gas concentration due to volumetric flow changes was accounted for. Radial temperature gradients within and between the monolith and the washcoat were neglected. However, heat transport resistance between the monolith and the surrounding quartz tube was included. The quartz tube itself was assumed to have constant temperature and heat losses to the surroundings were neglected. Physical properties, e.g. heat capacity, thermal conductivity and diffusivity, were assumed constant and estimated for an average gas composition at 300°C.

As the experimental space velocity was high (30 000 h^{-1}), it was found that mass and heat accumulation in the bulk gas could be neglected. Mass and heat balances were numerically calculated for the bulk gas, within the catalyst washcoat and in between the washcoat surface and the bulk gas. A heat balance for the quartz tube was also included. Further details regarding the reactor model are presented in Paper III.

4.2 Kinetic model

For the complete kinetic model a mean field model was used, consisting of 23 reactions. These reactions involved 7 gas phase species and 8 surface species on two types of catalytic sites, one for the hydrogen assisted HC-SCR reaction (*) and one for oxidation reactions (#). The surface species A, adsorbed on an SCR site (*), is marked A*, or A# if it is adsorbed on an oxidation site (#). The reaction steps are presented in Table 1-Table 4.

Surface reactions and adsorption/desorption processes were accounted for, treating surface reactions involving NOx adspecies as elementary reactions, while most other reactions are treated as overall reactions. The pre-exponential factors for adsorption were calculated from kinetic gas theory at the average temperature of 300°C, and the corresponding factors for desorption were set to 10^{13} s^{-1} [136]. The activation energy for adsorption of gaseous species was set to zero and the desorption activation energies for NO and O_2 were set to estimated values from the literature to reduce the number of parameters.

In the surface reactions involving NOx species on the SCR sites (*), adsorbed NO is oxidized both to surface nitrite (NO_2*) and nitrate (NO_3*) species, where NO_3* accumulates in the absence of hydrogen resulting in complete coverage of the SCR sites (*), thus preventing NOx

reduction. Gas phase hydrogen reacts with the NO_3* surface species, which are reduced to NO_2* surface species. This reaction with gas phase hydrogen, instead of adsorbed hydrogen, was included to clear the SCR sites (*) from nitrates (NO_3*), thereby gaining instantaneous NOx reduction at the introduction of hydrogen, as observed in the experiments. The n-octane hydrocarbon reacts with surface oxygen to form CH_2* surface species, representing various partially oxidized species proposed as reaction intermediates. The CH_2* species subsequently reduce NO_2* species to N_2. Direct NOx reduction by hydrogen was not included in the model as it has been shown in the literature that hydrogen does not act as a reducing agent alone, but as a strong promoter of the HC-SCR reaction. Nitrous oxide was neglected as the N_2O formation during the experiments always was low.

Adsorption/desorption and oxidation reactions, such as e.g. oxidation of n-octane by oxygen or NO_2 and direct oxidation of hydrogen, occur on the oxidation sites (#). The need for a second site was obvious as e.g. the oxidation of n-octane was observed during experiments in the absence of hydrogen, where the SCR sites (*) were completely covered by nitrates.

Further details concerning the kinetic model are presented in Paper III.

Table 1: Reactions and rate expressions for adsorption/desorption on HC-SCR sites (*)

	Reaction	Rate Expression
1	$NO + * \rightarrow NO*$	$r_1 = k_1 P_{NO*} \theta_*$
2	$NO* \rightarrow NO + *$	$r_2 = k_2 \theta_{NO*}$
3	$O_2 + 2* \rightarrow 2O*$	$r_3 = k_3 P_{O2} \theta_*^2$
4	$2O* \rightarrow O_2 + 2*$	$r_4 = k_4 \theta_{O*}^2$
5	$NO_2 + * \rightarrow NO_2*$	$r_5 = k_5 P_{NO2} \theta_*$
6	$NO_2* \rightarrow NO_2 + *$	$r_6 = k_6 \theta_{NO2*}$
7	$CO + * \rightarrow CO*$	$r_7 = k_7 P_{CO} \theta_*$
8	$CO* \rightarrow CO + *$	$r_8 = k_8 \theta_{CO*}$

Table 2: Reactions and rate expressions for NOx adspecies on HC-SCR sites (*)

	Reaction	Rate Expression
9	$NO* + O* \rightarrow NO_2* + *$	$r_9 = k_9 \theta_{NO*} \theta_{O*}$
10	$NO_2* + * \rightarrow NO* + O*$	$r_{10} = k_{10} \theta_{NO2*} \theta_*$
11	$NO_2* + O* \rightarrow NO_3* + *$	$r_{11} = k_{11} \theta_{NO2*} \theta_{O*}$
12	$H_2 + NO_3* \rightarrow H_2O + NO_2*$	$r_{12} = k_{12} \theta_{NO3*} P_{H2}$

Table 3: Reactions and rate expressions for surface reactions on HC-SCR sites (*)

	Reaction	Rate Expression
13	$C_8H_{18} + O^* + 7^* \rightarrow 8CH_2^* + H_2O$	$r_{13} = k_{13} P_{oct} \theta_{O^*}^2 \theta_*$
14	$CH_2^* + 2NO_2^* \rightarrow N_2 + CO^* + 2O^* + H_2O$	$r_{14} = k_{14} \theta_{CH2^*} \theta_{NO2^*}$
15	$CH_2^* + 2O^* \rightarrow CO^* + 2^* + H_2O$	$r_{15} = k_{15} \theta_{CH2^*} \theta_{O^*}$
16	$CO^* + O^* \rightarrow CO_2 + 2^*$	$r_{16} = k_{16} \theta_{CO^*} \theta_{O^*}$

Table 4: Reactions and rate expressions for adsorption/desorption and oxidation reactions on HC oxidation sites (#)

	Reaction	Rate Expression
17	$O_2 + 2\# \leftrightarrow 2O\#$	$r_{17} = k_{17} P_{O2} \theta_\#^2$
18	$2O\# \rightarrow O_2 + 2\#$	$r_{18} = k_{18} \theta_{O\#}^2$
19	$NO_2 + \# \rightarrow NO_2\#$	$r_{19} = k_{19} P_{NO2} \theta_\#$
20	$NO_2\# \rightarrow NO_2 + \#$	$r_{20} = k_{20} \theta_{NO2\#}$
21	$C_8H_{18} + 25\ O\# \rightarrow 8CO_2 + 25\# + 9H_2O$	$r_{21} = k_{21} P_{oct} \theta_{O\#}$
22	$C_8H_{18} + 25NO_2\# \rightarrow 8CO_2 + 25NO + 9H_2O + 25\#$	$r_{22} = k_{22} P_{oct} \theta_{NO2\#}$
23	$H_2 + O\# \rightarrow H_2O + \#$	$r_{23} = k_{23} \theta_{O\#} P_{H2}$

5 Results and discussion

5.1 Properties of the silver-alumina catalyst

The samples used in this work were thoroughly characterized by the methods presented in chapter 3. Explicit details of these analyses are presented in Paper I and Paper II. The nitrogen sorption measurements showed that the specific surface area of the samples varied between 142 - 213 m^2/g. However, the specific surface area generally decreased with increased silver loading, which is expected as high silver loading results in formation of a higher number of larger silver particles. This reduces the specific surface area as these silver particles are solid, in contrast to the highly porous alumina support. The silver particles may also block pores in the alumina matrix, which further reduces the specific surface area. This is shown in the results, as the extreme values presented above are the specific surface areas of a sample with 14 wt.% nominal silver loading (142 m^2/g, Paper II) and a sample nominally containing 2 wt.% silver (213 m^2/g, Paper I). The surface acidity is another important property of the catalyst for the HC-SCR reaction. Therefore, the surface OH-groups (Brønstedt acid sites) were characterized by *in-situ* DRIFT spectroscopy (Paper I). The stretching vibrations from surface hydroxyl groups are shown in the range of 3800-3650 cm^{-1} [137] and are dependent on the coordination to tetrahedral and/or octahedral alumina [137], which in turn affects the acidity. Our measurements showed no significant differences between the samples, neither in intensity (amount) nor position (strength) of the absorption bands for the OH stretching vibrations. These results indicate that the surface acidity does not offer an explanation for the differences in catalytic activity observed in this work.

In paper II, a thorough analysis of the silver content in the samples was performed by both SEM/EDX and ICP-SFMS. The results are presented in Table 5. As can be seen, the results differ between the methods, SEM/EDX showing slightly higher silver content for all samples, while the ICP/SFMS mainly shows lower silver content. The high silver content obtained by the SEM/EDX analysis is due to the relatively small area covered by the measurements, thus measuring the local silver loading. The ICP/SFMS analysis however, measures the global silver loading in a fraction of the sample.

5.1.1 Influence of preparation method

In Paper I, the influence of the preparation method on the characteristics of the silver-alumina catalyst was investigated. The X-ray diffraction patterns, shown in Figure 7, are obtained from samples with 5 wt.% nominal silver loading prepared according to the three different routes presented in Paper I. The impregnated sample (IM5) clearly shows diffraction peaks assigned to metallic silver (Ag^0) at $2\theta \approx 39$, 44, 64 and 77° (marked with circles). Further, the presence of crystalline silver-aluminate ($AgAlO_2$) is indicated by the double peak at $2\theta \approx$ 32-34° (square). However, none of these peaks are present for the sol-gel samples (SG5 and

Table 5: Silver loading (wt.%) according to SEM-EDXS and ICP-MS analysis, for the samples prepared in Paper II

	Silver loading (wt.%)									
Analysis method	*Impregnated samples*					*Freeze-dried sol-gel samples*				
Nominal silver loading (wt.%)	2.0	4.0	6.0	8.0	14.0	2.0	4.0	6.0	8.0	14.0
SEM-EDXS	3.4	5.4	6.3	9.4	16.7	3.4	4.6	7.7	9.5	16.1
ICP-SFMS	1.8	3.8	4.8	8.0	10.1	2.0	3.4	5.6	7.0	12.3

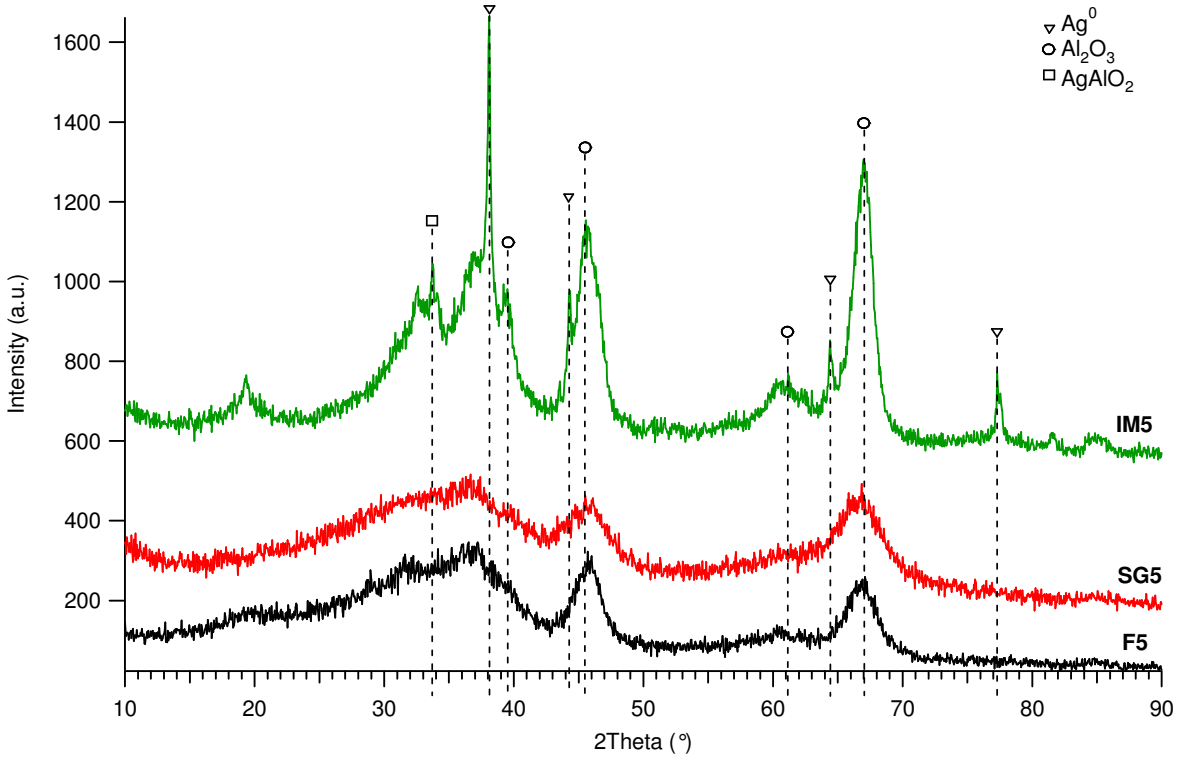

Figure 7: X-ray diffraction patterns for the impregnated (IM5), thermally dried sol-gel (SG5) and freeze-dried sol-gel (F5) samples, with 5 wt% nominal silver content. Peak assignments from She et al. [52] and the ICDD PDF-4+ database [138]. Triangles: Ag^0; circles: Al_2O_3; squares: $AgAlO_2$.

F5) and the peaks attributed to alumina (Al_2O_3, $2\theta \approx 39.5$, 45.5, 60 and 67°) are broad and diffuse for these samples. These observations support the presence of very small particles and/or an amorphous structure, both for the alumina and any silver containing species present in the samples. Comparing the broadening of the diffraction peaks, it can be concluded that the particle size in the sol-gel samples is several times smaller compared to the impregnated sample.

In Figure 8 the deconvoluted XPS spectra of the Ag $3d_{5/2}$ peak for the three different samples are presented. All samples show a shift in binding energy for the maximum of the $3d_{5/2}$ peak towards lower BE compared to metallic silver. For silver, contrary to most other elements, this shift towards lower BE indeed indicates a *higher* state of oxidation of the silver species on the sample surfaces [139-142]. However, after pre-reduction in 4 vol.% H_2 at 400 °C, the IM5 and SG5 samples show a clear shift of this peak to even lower BE. The deconvolution of the peak shows a higher proportion of AgO (shown as Ag^{2+} in Figure 8) for both samples after pre-reduction. This may be explained by the findings of Guo et al. [143], who showed that the position of the Ag $3d_{5/2}$ peak for very small silver clusters supported on alumina shifts towards higher BE when exposed to oxygen. The effect is pronounced upon heating to 427 °C, which is similar to the temperature of the pre-treatment procedure used in Paper I. The shift towards lower BE after reduction is thus an indication of the presence of small silver clusters on the surface of the IM5 and SG5 samples. The F5 sample, however, is considerably more stable and does not show a similar shift in BE. The deconvolution of the Ag $3d_{5/2}$ peak of the F5 sample shows a slightly higher fraction of Ag^{2+} for the pre-reduced sample than for the pre-oxidized sample. However, the number of clusters on the surface of this sample may be considered to be considerably lower than for the other samples, as no significant shift in BE can be observed.

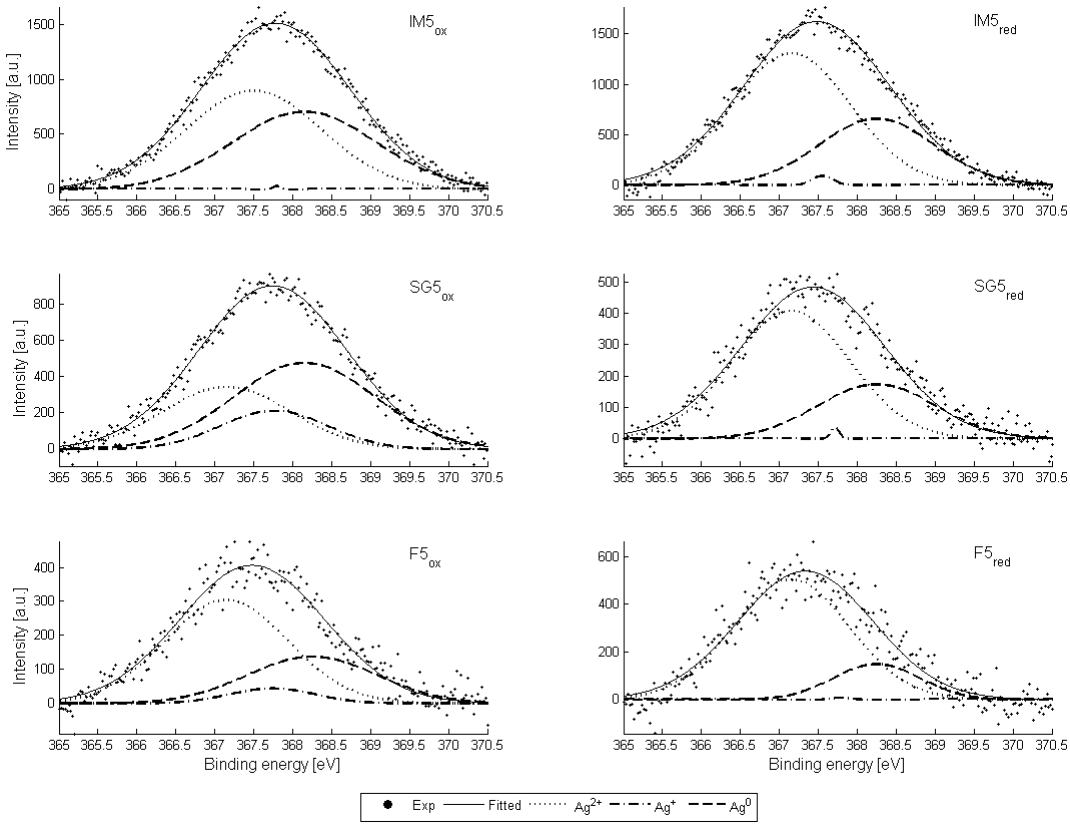

Figure 8: XPS spectra for the IM5, SG5 and F5 samples. The samples were pre-treated in 5% O_2 (ox) or 4% H_2 (red) at 400°C for 10 minutes and subsequently cooled in gas flow below 100°C. Gas flow: 300 ml/min, Ar bal. Experimental values are shown by dots; the fitted Gaussian peak is shown by a line. Deconvolution peaks: Ag^{2+} (AgO, dotted line), Ag^+ (Ag_2O, dash-dotted line) and Ag^0 (dashed line).

Complementary TEM micrographs of the same samples are shown in Figure 9. Compared to the sol-gel samples, the silver is clearly less dispersed in the impregnated sample, showing silver particles of around 20 nm in diameter. The particles in the sol-gel samples are commonly smaller, below 10 nm. Any significant differences in silver particle size between the sol-gel samples are difficult to observe. Nevertheless, the SG5 sample shows a higher number of particles than the F5 sample.

In summary, the results from the XRD, XPS and TEM analyses in Paper I suggest that the samples prepared by the sol-gel methods show a higher silver dispersion than the sample prepared by impregnation. Further, the XPS results suggest an even higher dispersion of silver in the freeze-dried sol-gel sample (F5).

5.1.2 Influence of silver loading

In Paper II, TEM techniques and O_2-chemisorption were used to determine the mean particle size (MPS) of samples with different silver loadings. Figure 10 shows bright field TEM and STEM/HAADF micrographs of samples prepared by the sol-gel method including freeze-drying, used in Paper II, with 2 and 6 wt.% silver loading. The micrographs show that the silver is unevenly distributed, with a silver particle size ranging between 5-20 nm. Also, free silver particles, not supported by the alumina, are observed. The mean particle size of samples with different silver loading, ranging from 2 wt.% to 14 wt.%, was determined by bright field TEM analyses.

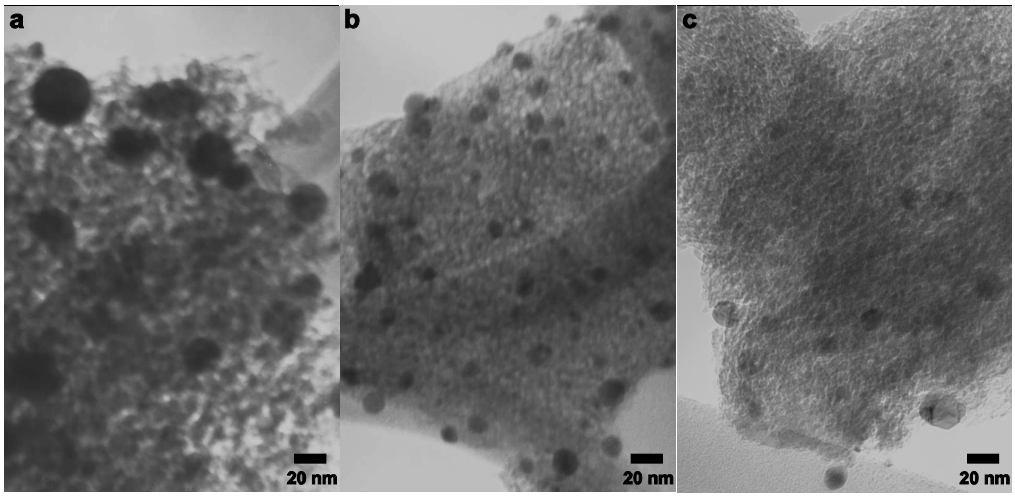

Figure 9: TEM micrographs of the IM5 (a), SG5 (b) and F5 (c) samples in Paper I.

The MPS of samples prepared by the impregnation method in Paper I, with similar silver loadings, was also determined. The results are presented in Table 6, showing quite similar MPS for all samples, although a slight difference depending on the preparation technique is noted. For samples containing ≥8 wt.% silver the MPS is somewhat higher for the impregnated samples. Further, it is noted that the free, unsupported particles increase in number with increasing silver loading for the sol-gel method, while this kind of particles are much less common in the impregnated samples. This is likely due to the EDTA/Ag complexes used in the impregnation method, as the complexes and the alumina support have opposite charges, thus facilitating attractive adsorption or ion exchange during the preparation procedure. To verify the results these samples were analyzed with STEM/HAADF, since the silver particles may be difficult to distinguish from the porous alumina structure, using bright field TEM. The results from the STEM/HAADF analysis were in accordance with the bright field TEM results, as shown in Figure 10.

As the TEM micrographs showed considerable local variations in silver particle size, O_2-chemisorption was applied to obtain not only the MPS, but also the global dispersion of silver, over a larger sample volume. As mentioned in chapter 3, the dispersion and particle size calculations are far from trivial, mainly because the Ag/O_2 stoichiometry is not known. In the literature, stoichiometries of 0.5, 2.0 and 4.0 have been proposed [46, 144, 145]. Further, in ref. [146] it is proposed that at low silver coverage, surface oxide $(Ag_2O)_s$ is formed, where the silver is in a monovalent oxidation state (Ag^+). However, at higher silver coverage other oxides are assumed to be formed, corresponding to a Ag/O ratio of 1 (i.e. $Ag/O_2 = 0.5$). These oxides

Table 6: Mean silver particle size according to TEM imaging and O_2-chemisorption (stoichiometry Ag/O_2=1), global dispersion according to O_2-chemisorption and fitted stoichiometry

	Sample (wt.%)									
Mean particle size	*Impregnated*					*Freeze-dried sol-gel*				
	2	4	6	8	14	2	4	6	8	14
TEM imaging (nm)	10.2	9.3	6.4	14.1	13.3	12.9	14.7	10.4	13.3	13.1
O_2-chemisorption (nm)	41.4	13.8	24.7	22.8	10.8	12.8	39.8	18.5	11.7	48.2
Global dispersion (%)	2.7	8.5	4.2	5.2	10.8	6.6	3.0	6.4	10.1	2.4
Fitted stoichiometry	4	1	4	1.5	0.75	1	2.5	2	1	4
Fitted dispersion (%)	10.8	8.5	16.8	7.8	8.1	6.6	7.5	12.8	10.1	9.6

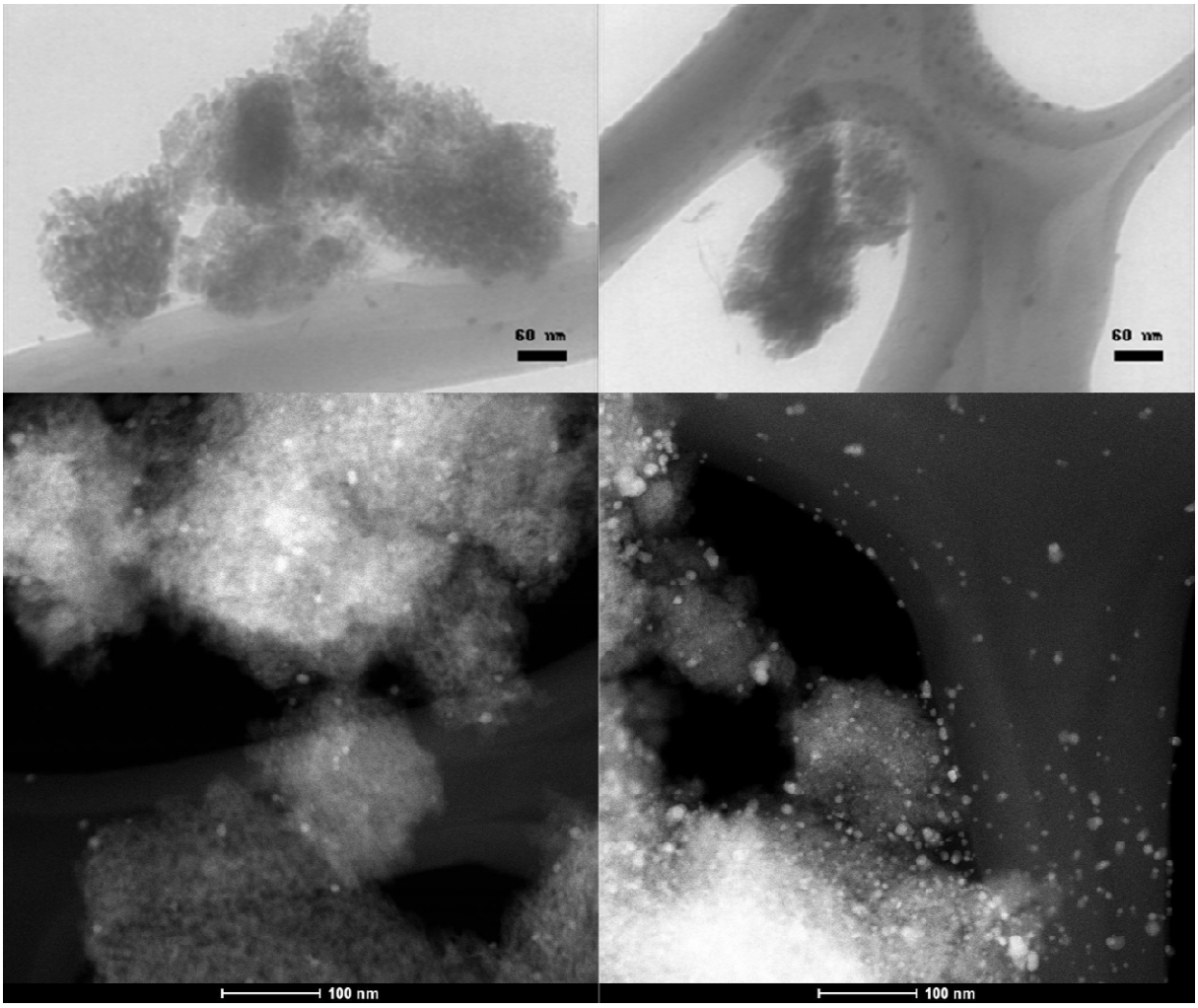

Figure 10: Bright field TEM (top) and STEM/HAADF (bottom) micrographs of the 2 wt.% (left) and 6 wt.% (right) freeze-dried sol-gel samples in Paper II.

involve either atomic oxygen anions (i.e. $(Ag_2O_2)_s$), or molecular oxygen of peroxide type [146]. It is therefore very likely that the Ag/O_2 stoichiometry changes with varying oxidation state of the silver. This is also influenced by the reduction of various surface silver phases in the samples. In Paper I it was shown by XPS that the freeze-dried sol-gel sample was unaffected by the reduction with 4 % hydrogen at 400 °C, while the impregnated sample was at least partially reduced. This supports the presence of strongly bound silver ions, which are hard to reduce, in samples with low silver loading, as suggested by Hoost et al. [46]. As a consequence, the silver dispersion may thus be underestimated. Also, the different preparation methods may cause formation of various types and/or amounts of silver phases, making the selection of reduction rate and temperature very difficult.

Both the reduction and O_2-chemisorption were performed consequently using the same experimental conditions for all samples, as described in Paper II. The stoichiometry $Ag/O_2=1$ was applied as a preliminary assumption, since a previous study by Arve et al. [144] showed that this value correlated best with results obtained by high resolution TEM/HAADF analysis. The results from the O_2-chemisorption are given in Table 6. In comparison to the results from the TEM analysis, the MPS clearly deviate, the O_2-chemisorption showing significantly higher MPS than the TEM imaging. Also between the preparation methods a difference in MPS can be observed, where the impregnated samples show a lower MPS, at least for the samples with

less than 8 wt.% silver loading. In Paper II, these differences are discussed more deeply. However, factors influencing the measurements may be the differences in specific surface area along with free and embedded silver particles. Due to the preparation method, the freeze-dried sol-gel samples very likely contain silver particles embedded in the alumina matrix, completely or partly. At the same time, it is observed in the TEM and STEM micrographs in Figure 10 that the freeze-dried sol-gel samples contain a significant amount of free silver particles. The chemical state of silver most probably differs between the free particles and the embedded silver. The embedded silver is likely oxidized and may not even be accessible for reduction prior to the O_2-chemisorption. The free silver particles on the other hand, are likely to be easily reduced, thereby in a metallic state during the chemisorption. This should have a significant impact on the Ag/O_2 stoichiometry.

A fitted stoichiometry was applied to calculate the stoichiometric factor corresponding to the mean particle size and dispersion values observed from TEM imaging (Table 6). As can be seen, the fitted Ag/O_2 stoichiometry varies significantly between 0.75 and 4, also resulting in non-integer values. These results clearly support the proposals made by Hoost et al. [46], that silver species with different oxidation states are present in the silver-alumina samples. This is also supported by the results obtained from the XPS analysis in Paper I.

5.2 Catalytic performance

This chapter concerns the performance of the prepared silver-alumina catalysts, with respect to catalytic activity, but also to the selectivity. Finally, aspects of the HC-SCR reaction over silver-alumina, focusing on the effect of hydrogen, are discussed.

Both the catalytic activity and selectivity are dependent on several factors, such as the type of reactor, space velocity, gas composition, temperature and of course type and number of active sites on the catalyst. As mentioned in chapter 3, two different reactor systems have been used to obtain kinetic data in this project. In Paper I and III a monolith reactor system was used, while the experiments in Paper II and V were performed using a powder reactor. The main difference between the monolith and powder reactor systems, given the same gas flow and catalyst volume, is the contact time between the feed gas and the catalyst surface, which both are considerably higher in the powder reactor than in the monolith reactor. This is due to the higher mass of catalyst for the same volume in the powder reactor. Also, the absence of defined channels increases the contact time in the powder bed. The increased contact time generally results in a higher activity in the powder reactor compared to the monolith reactor at similar space velocities.

The space velocity is defined as the hourly gas volumetric flow divided by the catalyst volume. However, the space velocity for the experiments performed using the powder reactor are based only on the volume of the active powder bed, whereas for the experiments performed with the monolith reactor also the open channel volume and the volume of the monolith substrate are included to calculate the space velocity. As the density of the active material is very different in these both cases, it is difficult to directly compare the space velocities. Therefore, a direct comparison of the activity tests is not straight forward. Moreover, as described in chapter 3.2 and detailed in the different papers, the instrumentation differed slightly between the reactor setups. Therefore, in Paper I and III, NOx conversion was measured, while N_2 formation (NO to N_2 reduction) was measured in Paper II and V. However, regarding the mechanistic discussion the trends are similar regardless of quantity.

Therefore, the expression "NOx conversion" is in this thesis used to describe both NOx conversion *per se*, but also the NO to N_2 reduction presented in Paper II and V.

5.2.1 Silver loading and dispersion vs. nature of the hydrocarbon

5.2.1.1 Paraffins and olefins

In Paper I, propene and n-octane were used as reducing agent for the HC-SCR reaction under dry conditions (i.e. without water added to the gas feed). The immediate difference observed between the two reducing agents is that for n-octane the NOx-conversion is generally higher at lower temperatures, as shown in Figure 11. This behavior correlates with the heat of adsorption of the hydrocarbon: For straight hydrocarbons, the heat of adsorption increases with the chain length on acidic zeolites [147, 148]. Further, for alkenes the heat of adsorption is higher than for the corresponding alkane [148]. However, due to the relatively long carbon chain length, the heat of adsorption is significantly higher for n-octane compared to propene [147, 148]. As alumina contains a large amount of acid sites, it is reasonable to assume a similar adsorbing behavior of the reducing agents over the silver-alumina catalysts compared to acidic zeolites, as suggested by Shimizu et al. [90]. Increased heat of adsorption indirectly indicates a higher sticking probability, i.e. that n-octane likely adsorbs and sticks more easily to the catalyst surface than propene, since this is more energetically favorable for n-octane. Another factor to consider regarding the low temperature activity is the terminal C-H bond strength of the hydrocarbon. To activate the hydrocarbon for the HC-SCR reaction, it needs to be partially oxidized [149]. Burch et al. [150] and Arve et al. [124] have suggested that the SCR mechanism includes dissociative chemisorption of the hydrocarbon, with the breaking of the terminal C-H bond as the rate determining step [124, 150]. In general, the C-H bond strength is a function of the position of the carbon atom in the molecule. As an example, a H–CH_2R bond (R is a general hydrocarbon chain) is generally stronger than a H–$CH(R_1)R_2$ bond (R_1, $R_2 \neq$ H) [151, 152]. This is clearly observed for propane in Table 7. Further, the ionization and deprotonation energies decrease with increasing length of the hydrocarbon chain [153]. This is due to the ability of the side groups to distribute the charge emerging from the breaking of the bond. In Table 7 and Table 8, a selection of terminal C-H bond strengths (Table 7) and ionization and deprotonation energies (Table 8) are presented. Following from the discussion above, n-octane is thus likely to adsorb on the catalyst surface at lower temperatures than propene. Hence, n-octane may be partially oxidized at lower temperatures compared to propene and subsequently react with adsorbed NOx species, reducing them to N_2.

Table 7: Bond energies of terminal C-H bonds for different hydrocarbons [151, 152]

Hydrocarbon	Bond	Bond energy (kJ/mol)
Propene	H-CH_2CHCH_2	362
Propane	H-n-C_3H_7	423
	H-i-C_3H_7	409
Benzene	H-C_6H_5	473
Toluene	H-$CH_2C_6H_5$	376
Cumene	H-$C(CH_3)_2$ C_6H_5	353
Cyclohexane	H-cyclohexyl	400
Methylcyclohexane[a]	H-$CH_2C_6H_{11}$	415 – 435

[a] Value approximately 40 – 60 kJ/mole (10 – 15 kcal/mole) higher than the corresponding bond for toluene due to less delocalization [151].

Table 8: Ionization and deprotonation energies for different hydrocarbons [153]

Hydrocarbon	Formula	Ionization energy (eV)	Deprotonation energy ΔH^o (kJ/mol)
Ethane	C_2H_6	11.5	1758
Propane	C_3H_8	10.9	1755
n-Butane	C_4H_{10}	10.5	1739
n-Pentane	C_5H_{12}	10.3	n/a
n-Hexane	C_6H_{14}	10.1	n/a
n-Heptane	C_7H_{16}	9.9	n/a
Cyclohexane	C_6H_{12}	9.9	1690
n-Octane	C_8H_{18}	9.8	n/a
Propene	C_3H_6	9.7	1636
Methylcyclohexane	C_7H_{14}	9.6	n/a
Benzene	C_6H_6	9.2	1681
Toluene	C_7H_8	8.8	1587
Cumene	C_9H_{12}	8.7	1585

However, the maximum conversion with n-octane as reductant is generally lower compared to propene. Also, for some samples the activity reaches a plateau for a certain temperature interval, before increasing more sharply to the maximum NOx conversion (Figure 11). A possible explanation for this may again be the higher heat of adsorption of n-octane, compared to propene. Shimizu et al. [90] have shown that adsorbed carbonates and carboxylates are formed on the catalyst surface during n-octane-SCR in the absence of water in the feed. These partially oxidized carbonaceous species block the surface from adsorption of e.g. NOx species, inhibiting the NOx reduction. As the temperature increases, the carbonaceous species are removed by further oxidation and the SCR activity increases until the temperature becomes high enough to facilitate the complete oxidation of most of the hydrocarbons, which results in suppression of the NOx reduction. As the heat of adsorption is considerably lower for propene than for n-octane [147, 148], no plateau in activity is observed for this reducing agent since no carbonaceous species are blocking the catalyst surface [90]. A higher terminal C-H bond strength of propene would also offer an explanation to the generally higher maximum activity, as the reducing agent reacts with oxygen to a higher extent only at elevated temperatures.

Comparing the NOx conversion for the samples prepared by sol-gel with freeze-drying, used in Paper I (F2, F5 and F8, black lines Figure 11), the general trend is similar for both reducing agents. Nevertheless, the results using propene as reducing agent stands out, as the maximum NOx conversion is almost the same for all freeze-dried sol-gel samples. The differences are found in the temperature for the maximum NOx conversion, decreasing with increased silver loading, and in the broadening of the NOx conversion temperature window with higher silver loading. In Paper I, this was taken as an indication of highly dispersed silver. In Figure 12 the XRD data for the samples prepared by sol-gel with freeze-drying, used in Paper II, are presented. The data show similar patterns for all samples, where only diffuse alumina peaks are observed even for the sample with a nominal silver loading of 14 wt.%. These samples are prepared by the same sol-gel method including freeze-drying as in Paper I, and may therefore be considered very similar to the corresponding samples presented in Paper I. These results, combined with the characterization results in Paper I, and also with the findings in Paper II, imply that silver is indeed highly dispersed in all of the freeze-dried sol-gel samples. From

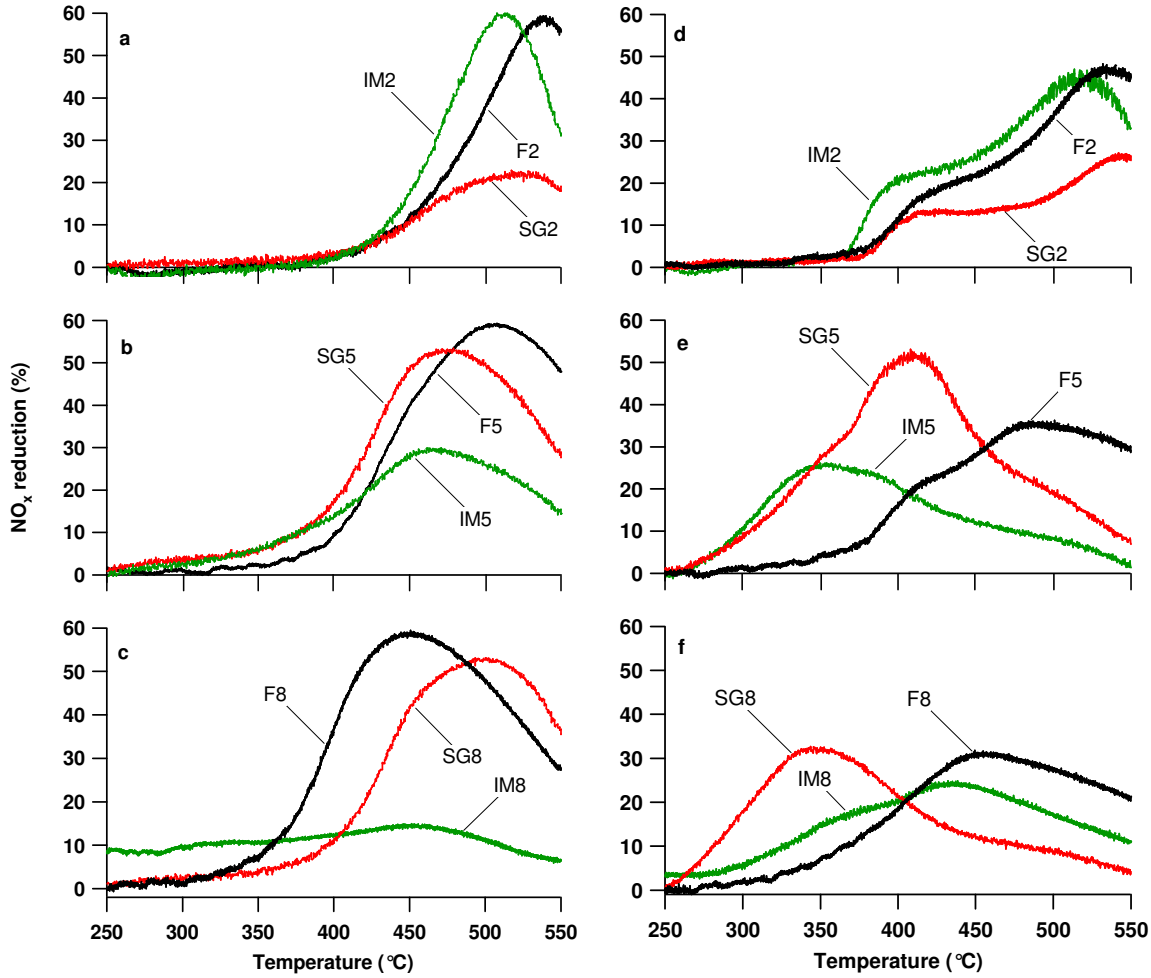

Figure 11: Reduction of NO_x with propene (a-c) or *n*-octane (d-f) as reducing agent for silver-alumina catalysts with nominal Ag content of 2 wt% (a, d), 5 wt% (b, e) and 8 wt% (c, f). The samples were prepared via the impregnation (IM), thermally dried sol-gel (SG) and sol-gel including freeze-drying (F) routes. Number index refers to the nominal silver content in the catalyst. Feed gas composition: 500 ppm NO, 500 ppm C_3H_6 (a-c) or 188 ppm C_8H_{18} (d-f), 5 % O_2, Ar bal. C/N ratio=3, GHSV: 30 000 h^{-1}.

Paper II, we know that the silver particle size is fairly constant, while the number of large (10-20 nm) particles increases with higher silver loading.

From the results for the 5 wt.% samples in Paper I, with n-octane as reducing agent (Figure 11e), it is readily observed that the SG5 sample shows the highest activity of the three samples. The maximum NOx conversion is very similar to the corresponding experiment with propene as reducing agent, but at 50 °C lower temperature. Also the activity window is much broader, with considerably higher NOx conversion in the temperature interval of 300-400 °C compared to propene. This is in line with the previous discussion about adsorption and activation of the reducing agent. However, it also indicates that the somewhat larger particles and/or the more easily reduced silver species in this sample, compared to the F5 sample, promote the reduction of NOx. The impregnated sample (IM5) contains even larger silver particles, showing high combustion of the reducing agent at lower temperatures. In Paper I the importance of the ratio between silver clusters and other oxidized silver species was stressed. However, following from the findings in Paper II and V, these results also indicate the crucial balance between silver sites and alumina sites, required for efficient NOx conversion. This will be discussed further in a following chapter.

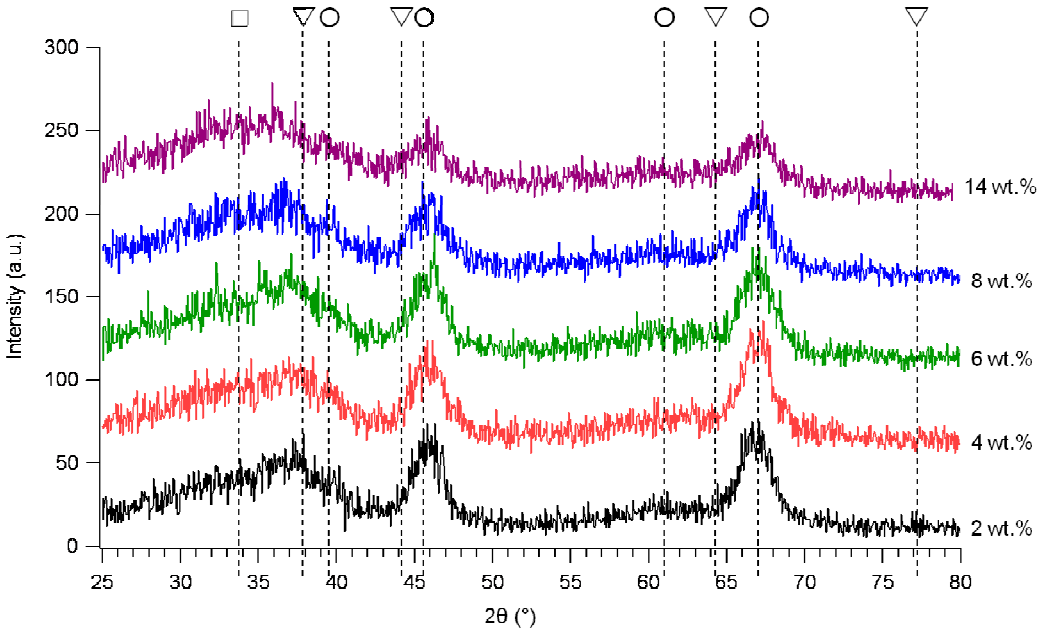

Figure 12: X-ray diffraction patterns for the silver-alumina samples prepared by sol-gel with freeze-drying, used in Paper II. Peak assignments from She et al. [52] and the ICDD PDF-4+ database [138]. Triangles: Ag^0; circles: Al_2O_3; squares: $AgAlO_2$.

5.2.1.2 Naphtenes and aromatic hydrocarbons

In Paper II, activity tests with naphtenes and aromatic hydrocarbons as the reducing agent for NOx were performed in a powder reactor (see Paper II for details). Also, the direct formation of N_2 was measured in this study. As pointed out in chapter 5.2, these two circumstances make a direct comparison between the activity tests in Paper I and Paper II somewhat difficult. However, the same general trends are still observed. It should be noted that in Paper II the NOx conversion results are presented as rate (mol s^{-1} m^2). However, for the reader to be able to easily compare the results in Paper I and Paper II, the NOx conversion results are presented in percent (%) in this thesis. The NOx conversion was calculated as

---

As mentioned in chapter 5.1, in Paper II several silver-alumina samples of different silver loading were prepared according to two different routes and characterized. However, after initial activity tests with n-octane, it was decided to proceed with only two samples, showing the most interesting results. These samples were prepared by the sol-gel method including freeze-drying (presented in Paper I), containing 2 and 6 wt.% silver.

The aim of the study presented in Paper II was to investigate the relationship between the nature of the reducing agent, silver loading and morphology and the activity (and selectivity) for NOx conversion. To achieve this, six different hydrocarbons were separately used as reducing agent in flow reactor activity tests: n-octane (as reference), methylcyclohexane, cyclohexane, benzene, toluene and cumene. The C/N ratio was kept constant at 6 for all experiments. The structures of the reducing agents are given in Figure 13. In Figure 14, the NOx conversion vs. temperature over the two silver-alumina samples is presented. The onset temperature with n-octane as reductant over the 2 wt.% and 6 wt.% samples was recorded approximately at the same temperature, however for the sample with lower silver loading the

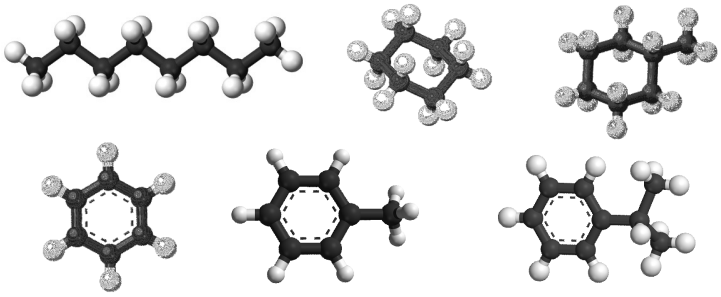

Figure 13: Structures of the reducing agents used in Paper II and V. Top: n-octane, cyclohexane and methylcyclohexane. Bottom: benzene, toluene and cumene.

NOx conversion was clearly higher and proceeded in a significantly broader temperature range than for the 6 wt.% catalyst. When the structure of the reducing agent was changed from linear to cyclic and aromatic, the maximum NOx reduction decreased over both catalysts and the onset temperature was shifted towards higher temperature in the following order: methylcyclohexane < cumene < cyclohexane < toluene < benzene. A similar behavior has previously been shown by Arve et al. [154], comparing the effects of n-octane, methylcyclohexane and toluene as reducing agents in the HC-SCR reaction over a 2 wt.% silver-alumina catalyst prepared by wet impregnation. Much more importantly however, the experimental results presented in this thesis (Paper II) showed that the onset temperature over the catalysts was shifted towards lower temperature with increasing silver content, when the aromatic reducing agent contains an alkyl group. The results strongly indicate that the NOx conversion over the catalyst is a combination between the nature of the reductant and the silver loading on the surface. In addition, the results provide support for the suggestion presented by Arve et al. [155], that the NOx conversion is not only a function of the hydrocarbon concentration, but also of its chain length, spatial arrangement and presence of functional groups. The same concept was also suggested in Paper I, where the importance of the ratio between silver clusters and other oxidized silver species was stressed.

The rate of heterogeneously catalyzed reactions depends on the rate constant and the coverage of reactants on the active sites, where the rate constant in turn is a function of the pre-exponential factor and the activation energy ($Ae^{-E_a/RT}$) [156]. Furthermore, the NO reduction over the catalysts studied in Paper II strongly depends on the nature of the reducing agent. Hence, it can be concluded that the activity is connected either to changes in the rate constant (i.e. the activation energy or the pre-exponential factor) or in the surface coverage of the reducing agent in relation to other adsorbed reactants, such as oxygen and NOx species. As mentioned previously, the terminal C-H bond strength, ionization and deprotonation energy differ between the different reducing agents (Table 7 and Table 8), which in turn affects the energy required to activate the hydrocarbon for further reaction as suggested in the literature [124, 150]. Furthermore, it is very likely that the structure of the reducing agent impacts the coverage of the hydrocarbon on the catalyst surface, as this affects the adsorption of the hydrocarbon. The size of the silver particles in the sample will also affect the adsorption of the hydrocarbon. However, over a certain particle size the amount of large silver particles is likely more important than the actual size. According to the TEM analysis (Figure 10 and Table 6), the amount of large silver particles increases with higher silver loading. Since the feed concentration of the hydrocarbon was kept constant over both catalysts, the differences in activity cannot be attributed only to the different terminal C-H bond energies, or different

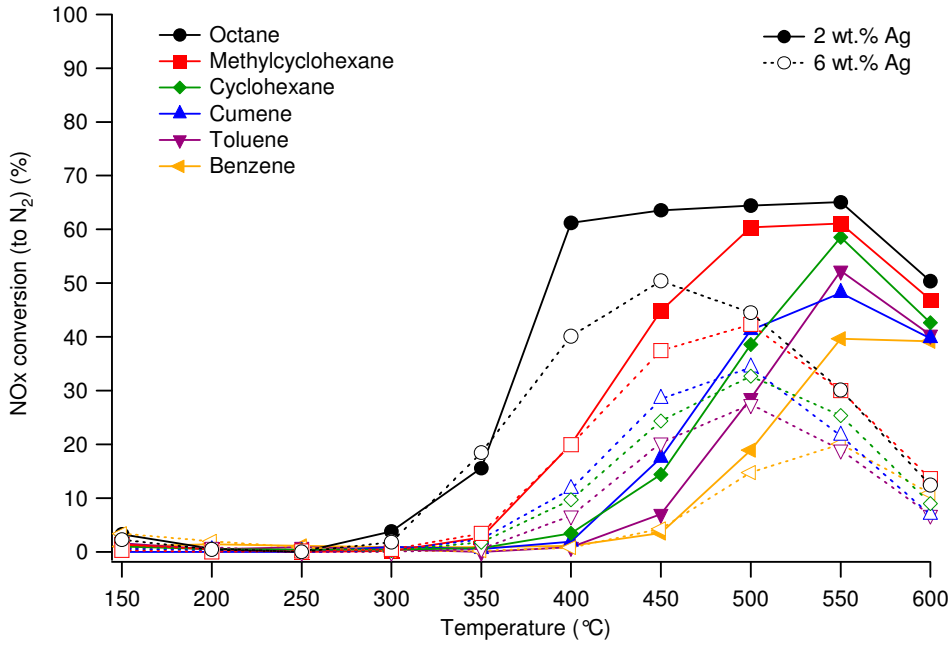

Figure 14: NOx conversion vs. temperature over the 2 wt.% (closed markers) and 6 wt.% (open markers, dashed line) silver-alumina samples prepared by sol-gel with freeze-drying, using octane (●,○) or methylcyclohexane (■,□) or cyclohexane (♦,◊) or cumene (▲,Δ)or toluene (▼,▽) or benzene (◄, ◁) as reducing agent. Gas feed: 500 ppm NO, 6 vol.% O_2, 10 vol.% CO_2, 350 ppm CO, 12 vol.% H_2O, He bal. C/N=6. Total flow: 500 ml/min. GHSV = 60 000 h^{-1}.

coverage due to the concentration changes in the feed gas. Thus, a reasonable explanation is that the coverage of hydrocarbon species depends on the size of the metal nanoparticles as reported in [157-163]. The overall activity of the HC-SCR reaction over silver-alumina likely depends both on the terminal C-H bond energy in the hydrocarbon as well as on the coverage of the hydrocarbon, which is influenced by the nature of the hydrocarbon molecule and the size of the silver particles. Further, the reactions between activated hydrocarbon and NOx species also depend on the type of reducing agent, as different N-containing species, such as amines etc. are formed [154], likely acting as intermediates in the HC-SCR reaction [149]. This indicates that different hydrocarbons may follow different paths in the HC-SCR reaction.

5.2.2 The influence of hydrogen addition and mechanistic aspects

In Paper III-V the influence of hydrogen addition to the gas feed is discussed. Paper III and IV focus on the reduction of strongly bound surface nitrates by hydrogen, confirming the observations of other groups [111, 115, 116, 164-166], by kinetic modeling (Paper III) and DRIFT spectroscopy studies (Paper IV).

Figure 15 shows the measured and calculated outlet concentrations of NO, NO_2, CO and CO_2, temperature and surface coverage, for two different transient (i.e. step-response) experiments with n-octane as reducing agent for the SCR reaction over silver-alumina. The experiments were performed at 250°C (transient series B) and 350°C (series C), as presented in Table 1 in Paper III. From the experimental results, the hydrogen effect is most apparent by comparing the first and second experiment in transient B (Figure 15, left). In the absence of hydrogen, no NOx reduction and only minor CO/CO_2 formation can be observed. However, after introduction of hydrogen, the reduction of NOx is observed almost instantly as a sharp decrease in the outlet NO_x concentration. Also the formation of CO/CO_2 and the outlet temperature increase dramatically when hydrogen is introduced.

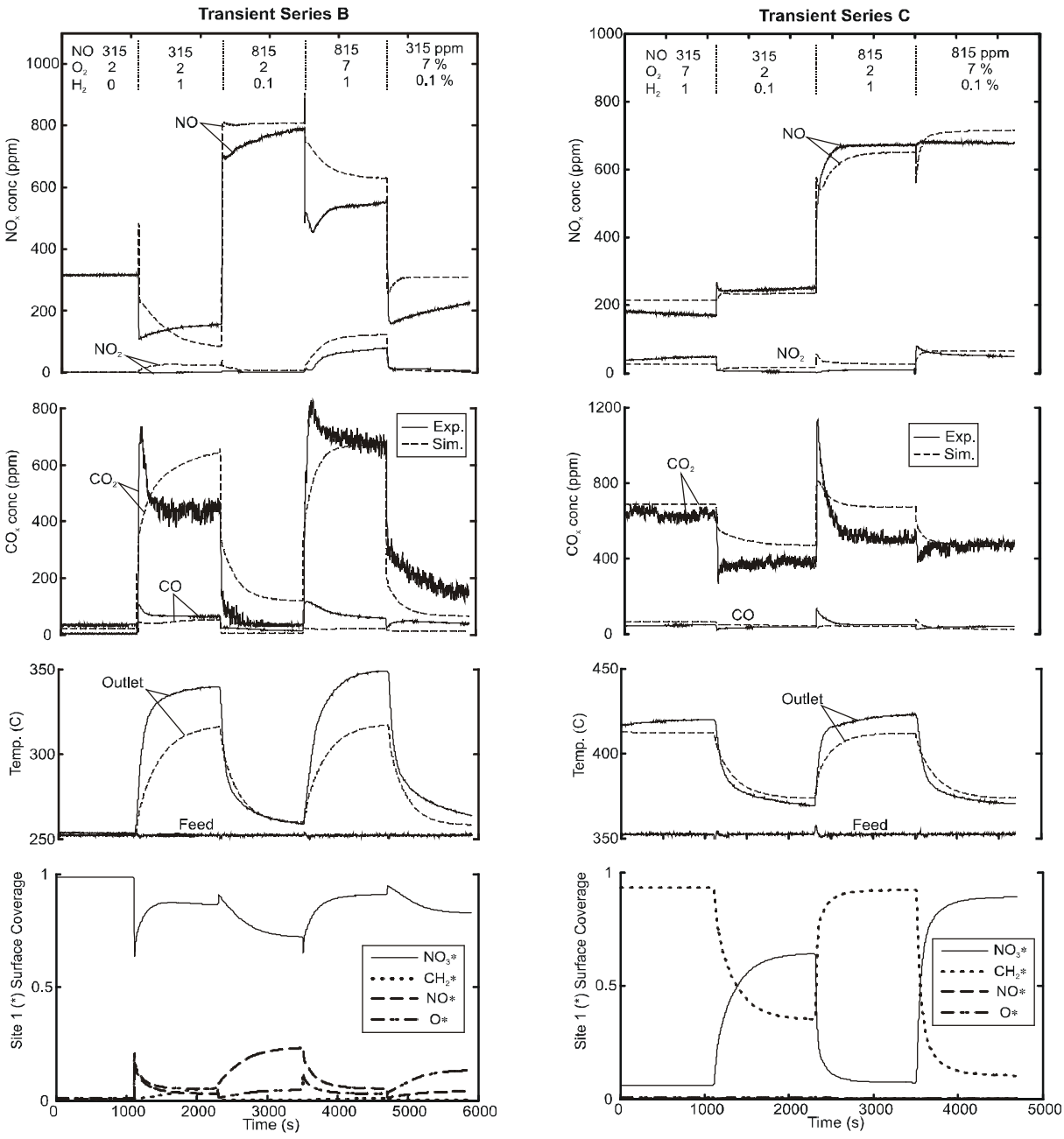

Figure 15: Transient series B (left) and C (right) (see Table 1 in Paper III) experimental and simulation results with varying feed concentrations of NO, O_2 and H_2. Constant feed conditions: 250°C (transient B), 350°C (transient C) and 150 ppm n-octane.

The mechanism behind the hydrogen effect has been discussed extensively in the literature. Hydrogen clearly promotes the HC-SCR reaction [25, 112, 164] and has been proposed to be involved in e.g. the activation of oxygen [116], of the reductant [115], or in the removal of nitrates poisoning the catalyst surface (see e.g. [115, 116]). The hydrogen is also reported to have an effect on the structure and state of the silver during the HC-SCR reaction (see e.g. [55, 112, 113]). As mentioned in chapter 4.2, the model used in Paper III uses the reduction of surface nitrates as a key feature. Comparing the experimental and simulated results in Figure 15, the simulated transient responses for the changes in NOx concentration and CO/CO_2 formation upon addition of hydrogen, are in the same timescale as the experimental results. This is true also for the response of the increase in the outlet temperature. The predicted steady state levels from the model coincide well for the experiments at 350°C (transient series

C, Figure 15, right), however not as good for the transients performed at 250°C (transient series B, Figure 15, left). Generally, the model follows the changes due to variations in the feed well, taking into account large temperature increases due to hydrogen combustion observed in the experiments. Also, some secondary effects by the removal of nitrates by hydrogen coincide with the other proposed effects [115, 116], mentioned above.

To further investigate the hypothesis with hydrogen breaking the self-poisoning of surface nitrates, DRIFT experiments were performed. In Paper IV, the evolution of surface NOx species was followed by DRIFT, after the removal of H_2 from a feed gas with either NO or NO_2, and O_2 (Figure 16). Upon introduction of NO or NO_2, O_2 and H_2 to the sample at 250 and 350°C, peaks around 1610, 1580 and/or 1560, 1540 and 1300 cm^{-1} evolve. In addition a peak at 1350 cm^{-1} is formed when NO_2 is used as NOx source. When H_2 is removed from the feed, all peaks increase in intensity. Absorption bands in the spectral regions 1650-1500 and 1300-1170 cm^{-1} are generally assigned to asymmetric stretching vibrations of nitrates on metal oxides (e.g. [85, 167]). Further, in a study not included in this thesis, first-principle calculations were used to assign surface NO_x species resulting from NO_2 adsorption on Ag/α-alumina [168]. A broad band in the range 1630-1590 cm^{-1} was assigned to weakly bound NO_2, bands between 1600 and 1460 cm^{-1} were attributed to surface nitrate species, while peaks in the range of 1440-1260 cm^{-1} were ascribed to surface nitrite species [168]. Hence, most likely the spectral features obtained in Paper IV arise from surface nitrite- and nitrate species, and in the 1610 cm^{-1} range also from weakly bound NO_2. However, as the peaks are broad and overlapping, further assignments of peaks are difficult [168].

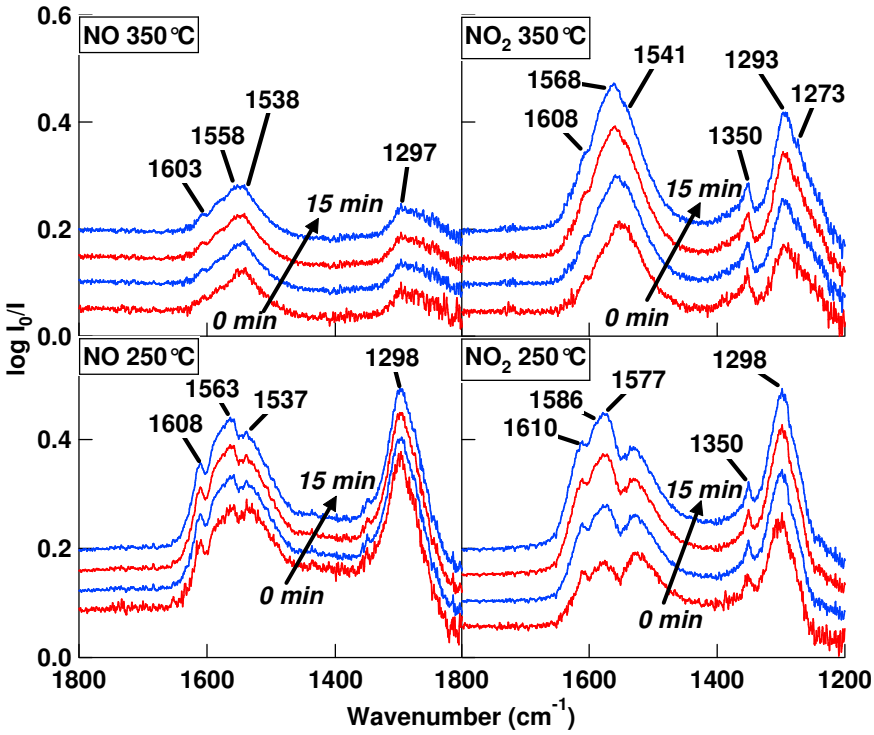

Figure 16: Evolution of NOx surface species after removal of 2000 ppm H_2 from the feed, during exposure to 1000 ppm NO (left) or NO_2 (right) and 8% O_2 (Ar bal.) at 350 °C (top) and 250 °C (bottom).

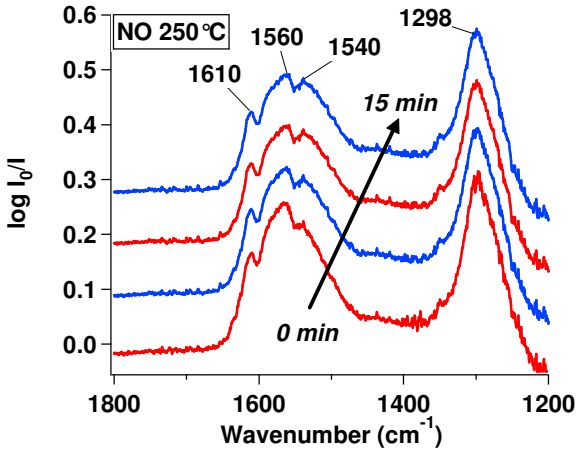

Figure 17: Reduction of NOx surface species after addition of 2000 ppm H_2 to the feed, during exposure to 1000 ppm NO and 8% O_2 (Ar bal.) at 250 °C.

Results from additional experiments, where H_2 instead was added to the feed (Figure 17), are in accordance with the results in Paper IV. When H_2 is added to the feed of NO and oxygen all peaks decrease in intensity, clearly showing reduction of the surface NOx species. In addition, water was formed during reaction with NO or NO_2 and H_2, in the presence of oxygen, which may be attributed to the reduction of surface nitrates to surface nitrites and water, albeit also to direct oxidation of hydrogen by oxygen. Nevertheless, these results strongly support the reduction of surface nitrates by hydrogen, which previously has been suggested to explain the promotional effect of hydrogen on the SCR of NOx over silver-alumina [111, 115, 116, 164-166]. Hydrogen may however also be involved in other steps in the SCR reaction.

In Paper V, the aim was to study the influence of hydrogen addition on the activity for HC-SCR of NOx over the same silver-alumina catalysts as in Paper II. The reducing agents used were also the same as in Paper II, i.e. n-octane, methylcyclohexane, cyclohexane, cumene, toluene and benzene, respectively. Figure 18 shows the NOx conversion over the 2 and 6 wt.% samples, with 1000 ppm hydrogen added to a gas feed consisting of 500 ppm NO, 6 vol.% O_2, 10 vol.% CO_2, 350 ppm CO and 12 vol.% H_2O, balanced by helium to a space velocity of 60 000 h^{-1}. The reducing agents were added maintaining C/N=6 in all experiments. The hydrogen effect is apparent in comparison to Figure 14, with much lower onset temperatures and increased activity at lower temperatures for both samples and all reductants. Maximum in NOx conversion is reached already at 300 °C and the conversion of NOx is then stable up to 550 °C. The complete oxidation of n-octane with oxygen at temperatures above 550 °C then results in a decrease in activity. For methylcyclohexane a dramatic increase in activity compared to Figure 14 can also be seen, even showing higher NOx conversion than n-octane at temperatures between 400-550 °C. For the aromatic hydrocarbons on the other hand, the NOx conversion increases almost linearly with temperature over the 2 wt.% sample in the current temperature range. This is in contrast to the volcano shaped activity curve observed for e.g. n-octane. However, the maximum NOx conversion is not shifted towards higher temperatures for the aromatic hydrocarbons, as it is reached at similar or lower temperatures in the presence of hydrogen (Figure 18) than without hydrogen (Figure 14). Instead, the NOx conversion is increased at lower temperatures, especially below 500 °C, when adding hydrogen to the feed. Cumene and toluene show very similar activity for the 2 wt.% sample over the entire temperature range. Only at 550 °C a significant difference in activity is observed where the

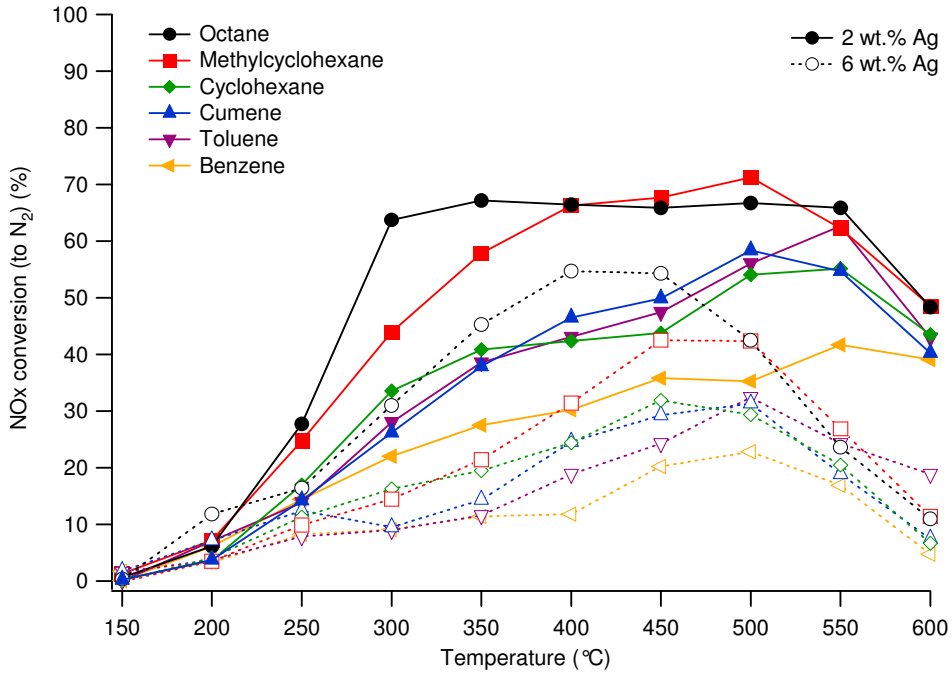

Figure 18: NOx conversion vs. temperature over the 2 wt.% (closed markers) and 6 wt.% (open markers, dashed line) silver-alumina samples prepared by sol-gel with freeze-drying, using octane (●,○) or methylcyclohexane (■,□) or cyclohexane (♦,◊) or cumene (▲,Δ)or toluene (▼,▽) or benzene (◄, ◁) as reducing agent. Gas feed: 500 ppm NO, 1000 ppm H_2, 6 vol.% O_2, 10 vol.% CO_2, 350 ppm CO, 12 vol.% H_2O, He bal. C/N=6. Total flow: 500 ml/min. GHSV = 60 000 h^{-1}.

cumene peak in activity at 500 °C, while toluene peaks at 550 °C. For benzene the activity increases with increasing temperature up to 550 °C, where the NOx reduction appears to reach its maximum. This behavior of the aromatic reducing agents over the 2 wt.% sample is interesting as it differs from the regular volcano shaped activity curve usually observed in the literature (e.g. [154]). This indicates that due to the addition of hydrogen and despite the constant C/N ratio, a high fraction of the hydrocarbon is available for SCR of NOx over the entire temperature range, especially at higher temperatures.

Concerning the NOx conversion over temperature over the 6 wt.% sample, compared to the results in Figure 14, it is readily observed that the maximum NOx conversion is shifted towards lower temperatures in most cases. The activity window is also broadened in a similar way as for the 2 wt.% sample. However, the maximum NOx conversion is still lower over the 6 wt.% sample than over the 2 wt.% sample. Thus it can be concluded that at higher temperatures (in the current temperature range) the undesired total oxidation of the hydrocarbon by oxygen does not occur to the same extent with these hydrocarbons over the 2 wt.% sample, as over the 6 wt.% catalyst.

In contrast to the experiments performed in absence of hydrogen in Paper II, the increase in activity at lower temperatures, due to higher silver loading, can no longer be observed for cyclohexane and toluene. However, an increased NOx reduction over the 6 wt.% sample is observed for both n-octane and cumene at 200 °C, compared to the 2 wt.% sample. Comparing the NOx activity at 200 °C over the two silver-alumina samples with the other reducing agents (i.e. methylcyclohexane, cyclohexane, toluene and benzene), the activity is generally higher over the 2 wt.% sample. This may be explained by nitrate poisoning of the surface and reduction of these surface nitrates by hydrogen, in combination with the nature of the reducing

agent. Nitrate poisoning of metallic silver is well known, and NOx species also adsorb on the silver-alumina surface, which likely results in self-poisoning at temperatures below 250 °C during HC-SCR conditions [41, 45, 64, 81, 169]. As shown in Paper III and IV, hydrogen may reduce the surface nitrates and possibly also surface nitrites. Thereby, sites required for the HC-SCR reaction may be available. However, as discussed in Paper V, the probability for the hydrogen to reduce sufficiently high amounts of the surface nitrates to free sites for adsorption and subsequent partial oxidation of hydrocarbons is likely higher over the 2 wt.% sample, as a consequence of the lower number of silver sites. This may then result in a higher N_2 formation. The higher activity over the 6 wt.% sample for n-octane and cumene as reducing agent is proposed to be due to the nature of the hydrocarbons. Comparing the ionization energies in Table 8, it is noted that cumene has lower ionization energy than benzene, indicating that cumene is easier to activate for reaction than benzene. However, n-octane has higher ionization energy than benzene, but the NOx conversion at 200 °C is nevertheless higher. This indicates that the activation of the hydrocarbon is influenced by other factors, one of which may be the adsorption of the hydrocarbon on the catalyst surface. Cumene may possibly adsorb by its propyl group and n-octane by one end of its chain, requiring fewer adjacent surface nitrates to be reduced by hydrogen than for example benzene, required to adsorb flat on the catalyst surface. Thus, partial oxidation of cumene and n-octane may occur to a higher extent over the 6 wt.% sample, resulting in a higher NOx conversion.

At temperatures above 200 °C, the activity is always higher for the 2 wt.% sample, which is suggested to depend on several factors. Hydrogen reduces adsorbed surface nitrates, as mentioned above. However, another (simultaneous) role of hydrogen is to enhance the partial oxidation of the hydrocarbon [55, 149], which explains the high NOx activity over the 2 wt.% sample for all reducing agents. As a result of the enhanced oxidation by hydrogen, fewer oxidation sites are required to activate the hydrocarbon reducing agent, also at lower temperatures, resulting in higher NOx conversion over this sample.

At 220 °C the nitrates adsorbed on the alumina support decompose to the gas phase [81]. However, the silver nitrates are more stable [41], decomposing at a higher temperature. This means that at 250 °C, the reduction of surface nitrates by hydrogen is still required to free sites for the adsorption of the hydrocarbon on the silver particles, resulting in a higher activity over the 2 wt.% sample as the number of silver nitrates is much lower than in the 6 wt.% sample. This is also indicated by the differences in activity of the different hydrocarbon reducing agents, where the terminal C-H bond energy and ionization energy (Table 7 and Table 8) are most likely important factors for the activity. Another reason for the lower activity over the 6 wt.% sample, compared to the 2 wt.% sample, is the blocking of alumina sites by silver. Alumina sites are required for different steps in the HC-SCR reaction. One example is the conversion of cyanide species into isocyanate species, shown by Bion et al. [62] and Thibault-Starzyk et al. [170], that requires adjacent silver and alumina sites to occur. According to Bion et al. [62], the isocyanate is then either hydrolyzed into ammonia, which subsequently reduces NO to N_2, or the isocyanate is oxidized into N_2 and CO_2. Regarding the crucial interaction between silver and alumina for this reaction step (and possibly others), it is most likely that the number of silver sites in the 6 wt.% sample is too high in relation to the number of alumina sites, to achieve a high NOx conversion. This might result in self-poisoning of the SCR-reaction by e.g. cyanide species at temperatures below peak NOx conversion, i.e. below 400 ° for n-octane and below 500 °C for the aromatic hydrocarbons over the 6 wt.% sample. Such self-

poisoning of cyanide, or other adsorbed species that require adjacent silver and alumina sites for further reaction, is likely the main reason for the lower NOx conversion over the 6 wt.% sample, at temperatures below the peak activity. At temperatures higher than the peak activity, the complete oxidation of the reducing agent by oxygen is instead promoted.

Furthermore, a difference between the NOx conversion and N_2 formation was observed in Paper V, indirectly indicating formation of other N-containing species, such as ammonia or amines, during the HC-SCR reaction. Formation of amines and ammonia is reasonable to assume, since such species were detected in other studies [154, 171, 172]. Arve et al. [154] showed the formation of amines at very similar conditions as for this study, although a significantly higher amount of hydrogen (1 vol.%) was added to the feed. Further, the formation of ammonia has also been shown, by e.g. DiMaggio et al. [172], but also in another study [171], not included in this thesis, at similar conditions as in Paper V. It is therefore reasonable to assume some formation of amines and ammonia over both samples. However, in ref. [171] it was found that a higher silver loading promotes the formation of ammonia. Thus, it is likely that the formation of amines is promoted over the 2 wt.% sample, and that ammonia formation is promoted over the 6 wt.% sample [154, 171, 172]. This supports the notion of different reaction paths for different hydrocarbons, as suggested previously.

6 Concluding remarks

A new preparation method for silver-alumina HC-SCR catalysts, based on sol-gel with freeze-drying of the formed gel, is presented. The characterization of the catalysts prepared by this method show that the samples are composed of very small particles with the silver finely distributed throughout the alumina matrix (Paper I). However, the samples also contain free silver particles, loosely bound to the alumina support (Paper II).

Flow reactor experiments show that the activation of the SCR reaction is highly dependent on the nature of the reducing agent (Paper I-II, V), but more interestingly also on the silver loading and distribution on the support. As the nominal silver loading was increased from 2 to 6 wt.% (Paper II) the SCR activity clearly increased at temperatures below 500 °C, when aromatic hydrocarbons containing alkyl groups or cyclohexane were used as reducing agents. The most reasonable explanation is that as the size and/or morphology of the silver particles on the alumina surface is changed, the coverage of different hydrocarbons change as well. Hence, different reducing agents result in varying NOx reduction, which depends on the silver loading and the nature of the hydrocarbon, i.e. most likely the terminal C-H bond strength and the heat of adsorption. Further, the balance between the number of oxidation- and reduction sites on the silver-alumina catalyst is of outmost importance and is dependent on the nature of the reducing agent. To achieve a high low-temperature activity using diesel fuel as the reducing agent, the ratio between oxidation- and reduction sites must be considered when designing the catalyst (Paper I-II, V).

A kinetic model for H_2-assisted *n*-octane-SCR of NOx over silver-alumina has been developed (Paper III). The formation of stable nitrates, poisoning the catalytic surface, subsequently reduced by hydrogen, is a key feature of the model. Changes due to variations in the feed are well reproduced in general. In particular poisoning effects of higher NO feed concentrations, presumably due to nitrate formation, and the strong promotion of the NOx reduction by hydrogen is well represented. Moreover, DRIFT results indicate the removal of surface nitrates in the presence of hydrogen (Paper IV). These results together leads to the conclusion that the removal of nitrates by hydrogen from the catalyst surface is one important feature of the hydrogen effect for HC-SCR over silver-alumina.

6.1 Outlook

The complete mechanism for HC-SCR over silver-alumina is still evading the scientific community, even though every new report adds to the common knowledge, incrementally bringing us closer and closer to a complete mechanism. The role of hydrogen has also become increasingly clear, although there are still questions, not easily answered.

One of the greatest tasks is to once and for all determine the active site (or sites) for the HC-SCR reactions. Proposals have been made, however consistent, undeniable proofs are yet to be presented. If this can be achieved, together with a clear understanding of the HC-SCR mechanism, a truly effective silver-alumina catalyst for HC-SCR of NOx may be designed. In this design the fuel penalty must be considered, as the fuel should be used as the reducing agent, but perhaps more importantly also for the production of hydrogen, required to achieve a high NOx reduction at low temperatures.

Acknowledgements

This work was performed as a part of the E4-Mistra program (Energy Efficient Reduction of Exhaust Emissions from Vehicles) within the Competence Centre for Catalysis (KCK). E4-Mistra is financially supported by Mistra (The Foundation for Strategic Environmental Research) and the Swedish Road Administration. KCK is financially supported by Chalmers University of Technology, the Swedish Energy Agency and the member companies: AB Volvo, Volvo Car Corporation, Scania CV AB, Saab Automobile Powertrain AB, Haldor Topsøe A/S and The Swedish Space Corporation. Financial support from Knut and Alice Wallenberg Foundation, Dnr KAW 2005.0055, is gratefully acknowledged.

I would also like to thank the following persons:

Professor **Krister Holmberg**, my examiner, for the opportunity to do research at Applied Surface Chemistry, and for great input, advice and support.

Professor **Magnus Skoglundh**, Director of KCK and my main supervisor. Thanks for all your comments, suggestions and pieces of advice. I'm especially grateful for your commitment, taking time whenever there is anything to discuss.

Associate professor **Hanna Härelind Ingelsten**, my second supervisor. I've said it before and I say it again: doing science would never be this fun without you! Thank you so much for being there for me, whenever I have wished for.

Docent **Kalle Arve**, Åbo Akademi University. It's a good thing to find a colleague, but it's much better to find a friend! Thanks for making my stay in Turku so great.

Professor **Dmitri Yu. Murzin** and docent **Kari Eränen**, Åbo Akademi University, for great scientific input and advice during my stay in Turku.

Akademiprofessor **Tapio Salmi**, Åbo Akademi University, for supporting my stay at the Laboratory of Industrial Chemistry and Chemical Engineering in Turku.

Professor **Eva Olsson**, professor **Derek Creaser**, associate professor **Henrik Grönbeck**, associate professor **Anders Hellman**, Dr **Jonas Sjöblom**, **Daniel Cederkrantz** and **Ma Yi** at Chalmers; Professor **Lasse Pettersson** and **Xanthias Karatzas** at the Royal Institute of Technology (KTH); **Jonas Edvardsson** and Dr **Miroslawa Abul-Milh** at Volvo Technology AB. Thank you for great cooperation and discussions.

Lars Lindström, for all the help in the reactor labs. How would anything work around there without you?

Dr **Elin** and **Lisa**, my whole and part officemates of past times. I'm a lucky guy to have you around!

Freddy, officemate and successor! Thanks for the great work as thesis and project worker, for talks about everything and simply the company.

Dr **Romain** for both serious but most of all unserious discussions.

All the people in the **E4-Mistra program** for great talks and cooperation.

Dr **Björn**, **Andreas**, Dr **Stefanie** and **Malin** for good company and all the help in the reactor lab and around.

Dr **Pierdomenico** for teaching me everything about fish and Italian wines, Dr **José Rafael** for showing me how to grill, and Dr **Atte** for taking my money.

All other friends at TYK and KCK for nice fikas and atmosphere.

Mum and Dad for all your encouragement since always.

Jenny, my wonderful wife, always by my side. Thank you for making my life so great! **Linnea**, my love, you have taken my heart and I never want it back.

List of abbreviations

BET	Brunauer-Emmett-Teller - Method for determination of surface area
BE	Binding energy
BJH	Barret-Joyner-Halenda - Method for determination of pore volume
DRIFTS	Diffuse reflectance infra-red Fourier transformed spectroscopy
EDX	Energy-dispersive X-ray spectroscopy
EGR	Exhaust gas recirculation
F#	Freeze-dried sol-gel sample (Paper I) with # wt.% silver loading
HAADF	High angle annular dark field
HC	Hydrocarbon
HRTEM	High resolution transmission electron microscopy
ICP	Inductively coupled plasma
IM#	Impregnated samples (Paper I) with # wt.% silver loading
IPCC	Intergovernmental Panel on Climate Change
MPS	Mean particle size
PM	Particulate matter
PGM	Platinum group metal
PSD	Pore size distribution
SCR	Selective catalytic reduction
SEM	Scanning electron spectroscopy
SFMS	Sector field mass spectroscopy
SG#	Thermally dried sol-gel sample (Paper I) with # wt.% silver loading
STEM	Scanning transmission electron spectroscopy
TEM	Transmission electron microscopy
TWC	Three-way catalyst
XPS	X-ray photoelectron spectroscopy
XRD	X-ray diffraction
ZSM5	Type of zeolite (Zeolite Socony Mobile 5)

References

[1] IPCC, *Climate Change 2007: The Physical Science Basis. Contribution of Working Group I to the Fourth Assessment Report of the Intergovernmental Panel on Climate Change*, Cambridge University Press: Cambridge, United Kingdom and New York, NY, USA, 2007.

[2] IPCC, *Climate Change 2007: Impacts, Adaptation and Vulnerability. Contribution of Working Group II to the Fourth Assessment Report of the Intergovernmental Panel on Climate Change*, Cambridge University Press: Cambridge, UK, 2007.

[3] IPCC, *Climate Change 2007: Mitigation. Contribution of Working Group III to the Fourth Assessment Report of the Intergovernmental Panel on Climate Change*, Cambridge University Press: Cambridge, United Kingdom and New York, NY, USA, 2007.

[4] E.V. Kondratenko, V.A. Kondratenko, M. Richter, R. Fricke, J. Catal. 239 (2006) 23.

[5] K. Shimizu, T. Higashimata, M. Tsuzuki, A. Satsuma, J. Catal. 239 (2006) 117.

[6] EEA, in: *Climate for a transport change - TERM 2007: indicators tracking transport and environment in the European Union*, 2008.

[7] K.C. Taylor, in: A. Crucq, A. Frennet (Eds.), *Catalysis and Automotive Pollution Control*, Elsevier Science Publishers B.V., Amsterdam, 1987, pp. 97-113.

[8] H.S. Ghandi, M. Shelef, in: A. Crucq, A. Frennet (Eds.), *Catalysis and Automotive Pollution Control*, Elsevier Science Publishers B.V., Amsterdam, 1987, pp. 199-214.

[9] *Bilavgasförordningen*, SFS 1987:586

[10] S.i. Matsumoto, CATTECH. 4 (2000) 102.

[11] A.E. Van Diepen, M. Makee, J.A. Moulijn, in: F.J.J.G. Janssen, R. A. van Santen (Ed.), *Environmental Catalysis*, Imperial College Press, London, 1999, pp. 257-291.

[12] C. Howitt, V. Pitchon, F. Garin, G. Maire, A. Frennet, J.M. Bastin, *Stud. Surf. Sci. Catal.*, Elsevier, 1995, pp. 149-161.

[13] K. Skalska, J.S. Miller, S. Ledakowicz, Sci. Total Environ. 408 3976.

[14] IPCC, in: S. Solomon, D. Qin, M. Manning, Z. Chen, M. Marquis, K.B. Averyt, M. Tignor and H.L. Miller (Ed.), *Climate Change 2007: The Physical Science Basis. Contribution of Working Group I to the Fourth Assessment Report of the Intergovernmental Panel on Climate Change*, Cambridge University Press, Cambridge, United Kingdom and New York, NY, USA, 2007, p. 212.

[15] United States Department of Transportations, (2010-07-12). http://www.bts.gov/publications/national_transportation_statistics/html/table_04_32b.html

[16] M. Zheng, G.T. Readerb and J.G. Hawley, Energy Convers. Manage. 45 (2004) 883.

[17] R. Burch, Cat. Rev. - Sci. Eng. 46 (2004) 271.

[18] M. Bowker, Chem. Soc. Rev. 37 (2008) 2204.

[19] E. Fridell, M. Skoglundh, B. Westerberg, S. Johansson, G. Smedler, J. Catal. 183 (1999) 196.

[20] Z.M. Liu, S.I. Woo, Cat. Rev. - Sci. Eng. 48 (2006) 43.

[21] M. Koebel, M. Elsener, M. Kleemann, Catal. Today. 59 (2000) 335.

[22] DieselNet, (2010-08-21). http://www.dieselnet.com/news/2010/03umicore.php

[23] E4MISTRA, in: *E4MISTRA Report Phase 1: 2006-2010*, H. Grönbeck (Ed.), 2010.

[24] DieselNet, (2010-07-12). http://www.dieselnet.com/standards/

[25] S. Satokawa, Chem. Lett. 29 (2000) 294.

[26] J.P. Breen, R. Burch, Top. Catal. 39 (2006) 53.

[27] R.M. Heck, R.J. Farrauto, with S.T. Gulati, *Catalytic Air Pollution Control*, 2 ed., John Wiley & Sons Inc.: New York, 2002.

[28] P.L.T. Gabrielsson, Top. Catal. 28 (2004) 177.

[29] V.I. Parvulescu, P. Grange, B. Delmon, Catal. Today. 46 (1998) 233.

[30] M. Iwamoto, H. Yahiro, Y. Yuu, S. Shundo, N. Mizuno, Shokubai. 32 (1990) 430.

[31] W. Held, A. Koenig, T. Richter, L. Puppe, SAE Paper. SP-810 (1990) 13.

[32] H. Hamada, Y. Kintaichi, M. Sasaki, T. Ito and M. Tabata, Appl. Catal. 75 (1991) L1.
[33] A. Obuchi, A. Ohi, M. Nakamura, A. Ogata, K. Mizuno and H. Ohuchi, Appl. Catal., B. 2 (1993) 71.
[34] R. Burch, J.P. Breen, F.C. Meunier, Applied Catalysis B: Environmental. 39 (2002) 283.
[35] T. Miyadera, Appl. Catal., B. 2 (1993) 199.
[36] N. Aoyama, K. Yoshida, A. Abe, T. Miyadera, Catal. Lett. 43 (1997) 249.
[37] K. Arve, F. Klingstedt, K. Eranen, D.Y. Murzin, L. Capek, J. Dedecek, Z. Sobalik, B. Wichterlova, K. Svennerberg, L.R. Wallenberg, J.O. Bovin, J. Nanosci. Nanotechnol. 6 (2006) 1076.
[38] K. Arve, L. Capek, F. Klingstedt, K. Eranen, L.E. Lindfors, D.Y. Murzin, J. Dedecek, Z. Sobalik, B. Wichterlova, Top. Catal. 30-31 (2004) 91.
[39] K. Arve, K. Svennerberg, F. Klingstedt, K. Eranen, L.R. Wallenberg, J.O. Bovin, L. Capek, D.Y. Murzin, J. Phys. Chem. B. 110 (2006) 420.
[40] K.A. Bethke, H.H. Kung, J. Catal. 172 (1997) 93.
[41] N. Bogdanchikova, F.C. Meunier, M. Avalos-Borja, J.P. Breen, A. Pestryakov, Appl. Catal., B. 36 (2002) 287.
[42] J.P. Breen, R. Burch, C. Hardacre, C.J. Hill, J. Phys. Chem. B. 109 (2005) 4805.
[43] M. Haneda, E. Joubert, J.C. Menezo, D. Duprez, J. Barbier, N. Bion, M. Daturi, J. Saussey, J.C. Lavalley, H. Hamada, Phys. Chem. Chem. Phys. 3 (2001) 1366.
[44] M. Haneda, E. Joubert, J.C. Menezo, D. Duprez, J. Barbier, N. Bion, M. Daturi, J. Saussey, J.C. Lavalley, H. Hamada, Phys. Chem. Chem. Phys. 3 (2001) 1371.
[45] A. Hellman, H. Grönbeck, Phys. Rev. Lett. 100 (2008) 116801.
[46] T.E. Hoost, R.J. Kudla, K.M. Collins, M.S. Chattha, Appl. Catal., B. 13 (1997) 59.
[47] A. Iglesias-Juez, M. Fernandez-Garcia, A. Martinez-Arias, Z. Schay, Z. Koppany, A.B. Hungria, A. Fuerte, J.A. Anderson, J.C. Conesa, J. Soria, Top. Catal. 30-31 (2004) 65.
[48] A. Iglesias-Juez, A.B. Hungria, A. Martinez-Arias, A. Fuerte, M. Fernandez-Garcia, J.A. Anderson, J.C. Conesa, J. Soria, J. Catal. 217 (2003) 310.
[49] L. Kylhammar, *Ag/Al_2O_3 catalysts for lean NOx reduction - synthesis, characterisation and activity studies*, Dept. Chemical and Biological Engineering, Chalmers University of Technology, Göteborg, 2005
[50] K. Luo, X. Lai, C.W. Yi, K.A. Davis, K.K. Gath, D.W. Goodman, J. Phys. Chem. B. 109 (2005) 4064.
[51] E. Seker, J. Cavataio, E. Gulari, P. Lorpongpaiboon, S. Osuwan, Appl. Catal., A. 183 (1999) 121.
[52] X. She, M. Flytzani-Stephanopoulos, J. Catal. 237 (2006) 79.
[53] C. Shi, M.J. Cheng, Z.P. Qu, X.H. Bao, Appl. Catal., B. 51 (2004) 171.
[54] K. Shimizu, J. Shibata, H. Yoshida, A. Satsuma, T. Hattori, Appl. Catal., B. 30 (2001) 151.
[55] K. Shimizu, M. Tsuzuki, K. Kato, S. Yokota, K. Okumura, A. Satsuma, J. Phys. Chem. C. 111 (2007) 950.
[56] K. Takagi, T. Kobayashi, H. Ohkita, T. Mizushima, N. Kakuta, A. Abe, K. Yoshida, Catal. Today. 45 (1998) 123.
[57] K. Shimizu, A. Satsuma, T. Hattori, Catal. Surv. Jpn. 4 (2000) 115.
[58] K. Arve, F. Klingstedt, K. Eranen, L.E. Lindfors, D.Y. Murzin, Catal. Lett. 105 (2005) 133.
[59] K. Arve, E.A. Popov, F. Klingstedt, K. Eranen, L.E. Lindfors, J. Eloranta, D.Y. Murzin, Catal. Today. 100 (2005) 229.
[60] K. Arve, E.A. Popov, M. Ronnholm, F. Klingstedt, J. Eloranta, K. Eranen, D.Y. Murzin, Chem. Eng. Sci. 59 (2004) 5277.
[61] H. Backman, J. Jensen, F. Klingstedt, J. Warna, T. Salmi, D.Y. Murzin, Appl. Catal., A. 273 (2004) 303.
[62] N. Bion, J. Saussey, M. Haneda, M. Daturi, J. Catal. 217 (2003) 47.

[63] N. Bion, J. Saussey, C. Hedouin, T. Seguelong, M. Daturi, Phys. Chem. Chem. Phys. 3 (2001) 4811.
[64] R. Brosius, K. Arve, M.H. Groothaert, J.A. Martens, J. Catal. 231 (2005) 344.
[65] G.W. Busser, O. Hinrichsen, M. Muhler, Catal. Lett. 79 (2002) 49.
[66] T. Chafik, S. Kameoka, Y. Ukisu, T. Miyadera, J. Mol. Catal. A: Chem. 136 (1998) 203.
[67] K. Eranen, F. Klingstedt, K. Arve, L.E. Lindfors, D.Y. Murzin, J. Catal. 227 (2004) 328.
[68] K. Eranen, L.E. Lindfors, F. Klingstedt, D.Y. Murzin, J. Catal. 219 (2003) 25.
[69] H.W. Gao, H. He, Q.C. Feng, J. Wang, Spectrochim. Acta, Part A. 61 (2005) 3117.
[70] H.W. Gao, H. He, Y.B. Yu, Q.C. Feng, J. Phys. Chem. B. 109 (2005) 13291.
[71] K.O. Haj, S. Ziyade, M. Ziyad, F. Garin, Appl. Catal., B. 37 (2002) 49.
[72] H. He, Y.B. Yu, Catal. Today. 100 (2005) 37.
[73] S. Kameoka, T. Chafik, Y. Ukisu, T. Miyadera, Catal. Lett. 55 (1998) 211.
[74] S. Kameoka, T. Chafik, Y. Ukisu, T. Miyadera, Catal. Lett. 51 (1998) 11.
[75] N. Kiattisirikul, C. Chaisuk, P. Praserthdam, Catal. Today. 97 (2004) 129.
[76] Z.P. Liu, S.J. Jenkins, D.A. King, JACS. 126 (2004) 7336.
[77] G. Madia, M. Koebel, M. Elsener, A. Wokaun, Industrial & Engineering Chemistry Research. 41 (2002) 4008.
[78] F.C. Meunier, J.P. Breen, V. Zuzaniuk, M. Olsson, J.R.H. Ross, J. Catal. 187 (1999) 493.
[79] F.C. Meunier, V. Zuzaniuk, J.P. Breen, M. Olsson, J.R.H. Ross, Catal. Today. 59 (2000) 287.
[80] F. Ouyang, R.S. Zhu, K. Sato, M. Haneda, H. Hamada, Appl. Surf. Sci. 252 (2006) 6390.
[81] V.A. Sadykov, V.V. Lunin, V.A. Matyshak, E.A. Paukshtis, A.Y. Rozovskii, N.N. Bulgakov, J.R.H. Ross, Kinet. Catal. 44 (2003) 379.
[82] A. Satsuma, K. Shimizu, Prog. Energy Combust. Sci. 29 (2003) 71.
[83] P. Sazama, L. Capek, H. Drobna, Z. Sobalik, J. Dedecek, K. Arve, B. Wichterlova, J. Catal. 232 (2005) 302.
[84] K. Shimizu, H. Kawabata, A. Satsuma, T. Hattori, Appl. Catal., B. 19 (1998) L87.
[85] K. Shimizu, H. Kawabata, A. Satsuma, T. Hattori, J. Phys. Chem. B. 103 (1999) 5240.
[86] K. Shimizu, J. Shibata, A. Satsuma, T. Hattori, Phys. Chem. Chem. Phys. 3 (2001) 880.
[87] S. Sumiya, H. He, A. Abe, N. Takezawa, K. Yoshida, J. Chem. Soc., Faraday Trans. 94 (1998) 2217.
[88] Q. Wu, H.W. Gao, H. He, Chin. J. Catal. 27 (2006) 403.
[89] Q. Wu, H. He, Y.B. Yu, Appl. Catal., B. 61 (2005) 107.
[90] K. Shimizu, A. Satsuma, T. Hattori, Appl. Catal., B. 25 (2000) 239.
[91] H.W. Gao, H. He, Spectrochim. Acta, Part A. 61 (2005) 1233.
[92] A. Abe, N. Aoyama, S. Sumiya, N. Kakuta, K. Yoshida, React. Kinet. Catal. Lett. 65 (1998) 139.
[93] A. Abe, N. Aoyama, S. Sumiya, N. Kakuta, K. Yoshida, Catal. Lett. 51 (1998) 5.
[94] T.N. Angelidis, S. Christoforou, A. Bongiovanni, N. Kruse, Appl. Catal., B. 39 (2002) 197.
[95] T.N. Angelidis, N. Kruse, Appl. Catal., B. 34 (2001) 201.
[96] V. Houel, P. Millington, S. Pollington, S. Poulston, R.R. Rajaram, A. Tsolakis, Catal. Today. 114 (2006) 334.
[97] F.C. Meunier, J.R.H. Ross, Appl. Catal., B. 24 (2000) 23.
[98] P.W. Park, C.L. Boyer, Appl. Catal., B. 59 (2005) 27.
[99] S. Satokawa, K. Yamaseki, H. Uchida, Appl. Catal., B. 34 (2001) 299.
[100] J. Wang, H. He, S.X. Xie, Y.B. Yu, Catal. Commun. 6 (2005) 195.
[101] S.X. Xie, Y.B. Yu, J. Wang, H. He, J. Environ. Sci.-China. 18 (2006) 973.
[102] T.N. Angelidis, V. Tzitzios, Appl. Catal., B. 41 (2003) 357.
[103] F. Bonet, S. Grugeon, R.H. Urbina, K. Tekaia-Elhsissen, J.M. Tarascon, Solid State Sci. 4 (2002) 665.
[104] H. He, J. Wang, Q.C. Feng, Y.B. Yu, K. Yoshida, Appl. Catal., B. 46 (2003) 365.

[105] A. Richter, M. Langpape, S. Kolf, G. Grubert, R. Eckelt, J. Radnik, A. Schneider, M.M. Pohl, R. Fricke, Appl. Catal., B. 36 (2002) 261.
[106] E.A. Sales, B. Benhamida, V. Caizergues, J.P. Lagier, F. Fievet, F. Bozon-Verduraz, Appl. Catal., A. 172 (1998) 273.
[107] K. Sato, T. Yoshinari, Y. Kintaichi, M. Haneda, H. Hamada, Catal. Commun. 4 (2003) 315.
[108] K. Sato, T. Yoshinari, Y. Kintaichi, M. Haneda, H. Hamada, Appl. Catal., B. 44 (2003) 67.
[109] J. Wang, H. He, Q.C. Feng, Y.B. Yu, K. Yoshida, Catal. Today. 93-95 (2004) 783.
[110] T. Miyadera, Appl. Catal., B. 13 (1997) 157.
[111] R. Burch, J.P. Breen, C.J. Hill, B. Krutzsch, B. Konrad, E. Jobson, L. Cider, K. Eranen, F. Klingstedt, L.E. Lindfors, Top. Catal. 30-31 (2004) 19.
[112] S. Satokawa, J. Shibata, K. Shimizu, S. Atsushi, T. Hattori, Appl. Catal., B. 42 (2003) 179.
[113] M. Richter, U. Bentrup, R. Eckelt, M. Schneider, M.M. Pohl, R. Fricke, Appl. Catal., B. 51 (2004) 261.
[114] H. Backman, J. Jensen, F. Klingstedt, T. Salmi, D.Y. Murzin, Appl. Catal., A. 294 (2005) 49.
[115] J. Shibata, K. Shimizu, S. Satokawa, A. Satsuma, T. Hattori, Phys. Chem. Chem. Phys. 5 (2003) 2154.
[116] K. Shimizu, J. Shibata, A. Satsuma, J. Catal. 239 (2006) 402.
[117] B. Wichterlova, P. Sazama, J.P. Breen, R. Burch, C.J. Hill, L. Capek, Z. Sobalik, J. Catal. 235 (2005) 195.
[118] D. Creaser, H. Kannisto, J. Sjöblom, H.H. Ingelsten, Accepted in Appl. Catal. B: Env. (2009)
[119] L.E. Lindfors, K. Eränen, F. Klingstedt, D.Y. Murzin, Top. Catal. 28 (2004) 185.
[120] R.K. Iler, *The Chemistry of Silica*, John Wiley & Sons, 1979, pp. 528-539.
[121] D.W. Johnson Jr, P.K. Gallagher, F.J. Scnettler, E.M. Vogel, Ceram. Bull. 56 (1977) 785.
[122] J. Dawody, M. Skoglundh, S. Wall, E. Fridell, J. Mol. Catal. A: Chem. 225 (2005) 259.
[123] M. Skoglundh, H. Johansson, L. Lowendahl, K. Jansson, L. Dahl, B. Hirschauer, Appl. Catal., B. 7 (1996) 299.
[124] K. Arve, F. Klingstedt, K. Eränen, J. Wärnå, L.E. Lindfors, D.Y. Murzin, Chem. Eng. J. 107 (2005) 215.
[125] J.R. Anderson, K.C. Pratt, *Introduction to Characterization and Testing of Catalysts*, Academic Press, North Ryde, N.S.W., 1985, pp. 2-6.
[126] S. Brunauer, Emmet P. H., Teller E., JACS. 60 (1938) 309.
[127] S. Brunauer, P.H. Emmett, E. Teller, J. Am. Chem. Soc. 60 (1938) 309.
[128] E.P. Barrett, L.G. Joyner, P.P. Halenda, J. Am. Chem. Soc. 73 (1951) 373.
[129] J.R. Anderson, K.C. Pratt, *Introduction to Characterization and Testing of Catalysts*, Academic Press, North Ryde, N.S.W., 1985, pp. 64-80.
[130] I. Chorkendorff, J.W. Nietmantsverdriet, *Concepts of Modern Catalysis and Kinetics*, Student ed., WILEY-WCH Verlag GmbH & Co, Weinheim, 2003, pp. 134-139.
[131] J. Thomas, P. Midgley, ChemCatChem. 2 (2010) 783.
[132] N. Ravishankar, J. Phys. Chem. Lett. 1 (2010) 1212.
[133] J.W. Niemantsverdriet, *Spectroscopy in Catalysis: An Introduction*, 2nd ed., Wiley-VHC Verlag GmbH: Weinheim, 2000.
[134] J.R. Anderson, K.C. Pratt, *Introduction to Characterization and Testing of Catalysts*, Academic Press: North Ryde, N.S.W., 1985.
[135] G. Busca, Catalysis Today. 27 (1996) 323.
[136] D.F.R. J.A. Dumesic, L.M. Aparicio, J.E. Rekoske, A.A. Trevino, *The Microkinetics of Heterogeneous Catalysis*, American Chemical Society, Washington DC, 1993, p. 40.
[137] H. Knözinger, P. Ratnasamy, Cat. Rev. - Sci. Eng. 17 (1978) 31.
[138] JCPDS - International Centre for Diffraction Data, Philadelphia, USA, 2007.

[139] M. Bielmann, P. Schwaller, P. Ruffieux, O. Groning, L. Schlapbach, P. Groning, Phys. Rev. B. 65 (2002) 235431.
[140] J.F. Weaver, G.B. Hoflund, J. Phys. Chem. 98 (1994) 8519.
[141] G. Schön, Acta Chem. Scand. 27 (1973) 2623.
[142] J.F. Moulder, W. F. Stickle, P. E. Sobol, K. D. Bomben, *Handbook of X-Ray Photoelectron Spectroscopy*, Perkin Elmer Corporation - Physical Electronics Division: Eden Prairie, 1992.
[143] D. Guo, Q. Guo, K. Zheng, E.G. Wang, X. Bao, J. Phys. Chem. C. 111 (2007) 3981.
[144] K. Arve, K. Svennerberg, F. Klingstedt, K. Eränen, L.R. Wallenberg, J.O. Bovin, L. Capek, D.Y. Murzin, J. Phys. Chem. B. 110 (2006) 420.
[145] G.I. Golodets, *Heterogeneous Catalytic Reactions Involving Molecular Oxygen*, Vol. 15; Elsevier: Amsterdam, The Netherlands, 1983.
[146] G.I. Golodets, *Stud. Surf. Sci. Catal.*, Elsevier, 1983, pp. 41-103.
[147] J.F. Denayer, G.V. Baron, J.A. Martens, P.A. Jacobs, J. Phys. Chem. B. 102 (1998) 3077.
[148] P. Pantu, B. Boekfa, J. Limtrakul, J. Mol. Catal. A: Chem. 277 (2007) 171.
[149] K. Eränen, F. Klingstedt, K. Arve, L.E. Lindfors, D.Y. Murzin, J. Catal. 227 (2004) 328.
[150] R. Burch, P. Fornasiero, T.C. Watling, J. Catal. 176 (1998) 204.
[151] G.B. Ellison, G.E. Davico, V.M. Bierbaum, C.H. DePuy, Int. J. Mass Spectrom. Ion Processes. 156 (1996) 109.
[152] D.R. Lide (Ed.), CRC Handbook of Chemistry and Physics, 80th ed., CRC Press LLC, Boca Raton, 1999.
[153] NIST - National Institute of Standards and Technology, (2010-09-15). http://webbook.nist.gov/chemistry/
[154] K. Arve, H. Backman, F. Klingstedt, K. Eränen, D.Y. Murzin, Appl. Catal. B: Environ. 70 (2007) 65.
[155] K. Arve, J.R.H. Carucci, K. Eränen, A. Aho, D.Y. Murzin, Appl. Catal. B: Environ. 90 (2009) 603.
[156] M. Bowker, *The Basis and Applications of Heterogeneous Catalysis*, Oxford University Press: Oxford, 1998.
[157] A.T. Bell, Science. 299 (2003) 1688.
[158] C.R. Henry, Appl. Surf. Sci. 164 (2000) 252.
[159] D.Y. Murzin, Langmuir. 26 (2009) 4854.
[160] R. Narayanan, M. El-Sayed, Top. Catal. 47 (2008) 15.
[161] J.R. Rostrup-Nielsen, J. Catal. 27 (1972) 343.
[162] R. Schlögl, S.B.A. Hamid, Angew. Chem. Int. Ed. 43 (2004) 1628.
[163] R.A. Van Santen, Acc. Chem. Res. 42 (2008) 57.
[164] K. Arve, H. Backman, F. Klingstedt, K. Eranen, D.Y. Murzin, Appl. Catal., A. 303 (2006) 96.
[165] H. Backman, K. Arve, F. Klingstedt, D.Y. Murzin, Appl. Catal., A. 304 (2006) 86.
[166] U. Bentrup, M. Richter, R. Fricke, Appl. Catal., B. 55 (2005) 213.
[167] S. Kameoka, Y. Ukisu, T. Miyadera, Phys. Chem. Chem. Phys. 2 (2000) 367.
[168] H.H. Ingelsten, A. Hellman, H. Kannisto, H. Grönbeck, Submitted to J. Catal. (2008)
[169] R. Burch, J.P. Breen, F.C. Meunier, Appl. Catal., B. 39 (2002) 283.
[170] F. Thibault-Starzyk, E. Seguin, S. Thomas, M. Daturi, H. Arnolds, D.A. King, Science. 324 (2009) 1048.
[171] H. Kannisto, X. Karatzas, J. Edvardsson, L.J. Pettersson, H.H. Ingelsten, *in preparation*, 2010.
[172] C.L. DiMaggio, G. B. Fisher, K. M. Rahmoeller, M. Sellnau, SAE Special publication. SP-2254 (2009) 47.